ARMY RESEARCH LABORATORY

A Numerical Study of the Injector Region of the 30-mm Regenerative Liquid Propellant Gun

by S. E. Ray

ARL-CR-336 September 1997

prepared by

Army High Performance Computing Research Center
and Aerospace Engineering and Mechanics
University of Minnesota

under contract

DAAH04-95-C-0008

The findings in this report are not to be construed as an official Department of the Army position unless so designated by other authorized documents.

Citation of manufacturer's or trade names does not constitute an official endorsement or approval of the use thereof.

Destroy this report when it is no longer needed. Do not return it to the originator.

Army Research Laboratory
Aberdeen Proving Ground, MD 21005-5066

ARL-CR-336 **September 1997**

A Numerical Study of the Injector Region of the 30-mm Regenerative Liquid Propellant Gun

S. E. Ray
Army High Performance Computing Research Center and Aerospace Engineering and Mechanics

prepared by

Army High Performance Computing Research Center
and Aerospace Engineering and Mechanics
University of Minnesota

under contract

DAAH04-95-C-0008

Abstract

A numerical study of the flow of liquid propellant (LP) in a regenerative LP gun (RLPG) is described. The model simulates the flow of LP from the liquid reservoir, through the orifice, and into the combustion chamber. The model is based on a space-time finite element method and can automatically handle the deformation of the computational domain. A mesh-moving scheme is used to update the mesh at every time step.

Two shots of the 30-mm RLPG are studied. One is a small-charge shot, and the other is a medium-charge shot. The results from the simulations compare well with data from another numerical model of the RLPG and with experimental data. The simulations provide qualitative details of the transient phenomena that occur in the orifice during the firing cycle. The agreement of the results from the model with experimental data provide confidence in the accuracy of the model. The numerical model will be used to study several RLPG shots under a variety of conditions.

Acknowledgments

The author would like to thank Ms. Gloria Wren and Dr. Terence Coffee of the U.S. Army Research Laboratory (ARL) and Dr. Tayfun Tezduyar of the Army High Performance Computing Research Center (AHPCRC), University of Minnesota for their assistance and insight. The author would also like to thank Mr. John Knapton and Dr. Paul Weinacht for reviewing the manuscript. The report is far better because of their suggestions.

This work is sponsored in part by AHPCRC under the auspices of the Department of the Army, ARL cooperative agreement number DAAH04-95-2-0003/contract number DAAH04-95-C-0008, the content of which does not necessarily reflect the position or the policy of the government, and no official endorsement should be inferred.

INTENTIONALLY LEFT BLANK.

Table of Contents

INTENTIONALLY LEFT BLANK.

List of Figures

1. Introduction

The regenerative liquid propellant gun (RLPG) is being studied by the U.S. Army as an advanced technology for future gun systems. There are several technical issues that must be resolved before RLPG technology is sufficiently mature for a fielded weapon system. In order to help researchers understand the gun's firing cycle sufficiently to solve the technical challenges presented by the RLPG, 30-mm, 105-mm and 155-mm RLPGs have been built and tested. In addition, a great deal of numerical modeling of the firing cycle has been performed in support of this goal.

The firing cycle of the concept VIC (6-C) RLPG begins with the liquid propellant (LP) stored in a liquid reservoir (see Figure 1). There are two pistons: (1) the inner, or control, piston, which moves along the centerline of the gun; and (2) the outer, or injection, piston, which surrounds the inner piston. An external ignitor injects hot gas into the combustion chamber to start the firing cycle. As the pressure in the chamber increases, the pistons are driven toward the breech. There is a damper that sits behind the control piston and slows the piston near the end of stroke. Early in the firing cycle, the damper applies relatively little force to the control piston, while, at the same time, the motion of the injection piston is slowed by the presence of LP in the reservoir. Therefore, the control piston moves a little faster, early in the firing cycle, than the injection piston, and the difference in the motion of the pistons opens an annular orifice between the pistons.

Throughout most of the firing cycle, the ratio between the pressure in the reservoir and the pressure in the chamber is equal to the inverse of the ratio between the effective areas over which the pressures act on the injection piston. In other words, the force that the chamber pressure exerts on the injection piston is roughly equal to the force that the reservoir pressure exerts on the piston. Since the ratio of the area on the chamber side to the area on the reservoir side is 1.47 for the 30-mm RLPG, the pressure in the reservoir is roughly 1.47 times the pressure in the chamber during most of the firing cycle. The higher pressure in the reservoir drives the LP from the reservoir through the orifice and into the

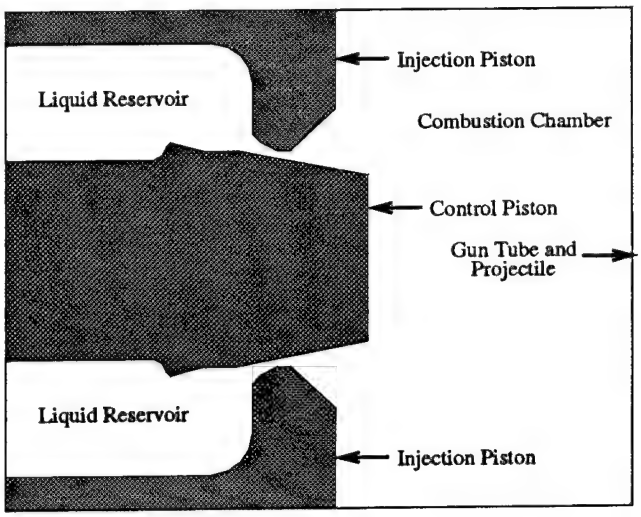

Figure 1. Sketch of the Concept VIC RLPG.

combustion chamber. The LP combusts in the chamber, accelerating the projectile down the gun tube.

Occasionally, the firing cycle does not proceed properly. The injection piston will slow or reverse its direction of travel before the end of stroke. This is called a piston hesitation or reversal, or simply a reversal. Not all causes of reversals have been identified. One cause may be combustion in the orifice or reservoir, and reversals of this type are the focus of this work. The source of the combustion in the reservoir is not known, although one possibility is a disruption of the flow in the orifice.

In order to test this hypothesis, a better understanding of the flow of LP in the orifice is needed. For instance, it is not yet known if the flow separates from the surface of the pistons, and what conditions cause this flow separation. As a part of the study of the RLPG firing cycle, a 30-mm RLPG was built and studied [1] and is still used as a tool in the study of the RLPG firing cycle. While the 30-mm RLPG is a very valuable experimental fixture, it is prohibitively difficult to measure enough experimental data in the orifice to describe the flow phenomena that occur there.

With the limitations that exist on the experimental study of the gun, it is necessary that numerical modeling provide at least a qualitative description of the flow phenomena that

occur during the firing cycle. Numerical modeling has been used to study the firing cycle of the RLPG for a number of years. Work by Coffee et al. [1–6] has been focused primarily in two areas. The first is the lumped parameter modeling of the RLPG firing cycle. The second involves modeling the combustion chamber.

In the lumped parameter approach, the spatial variations of the pressure, density, and temperature within both the reservoir and the chamber are neglected. Also, the flow through the orifice is computed using an assumption of Bernoulli flow [1]. While the data from the lumped parameter model match the experimental data very well and are very valuable to researchers, they do not provide many more details of the flow phenomena in the orifice than the experimental data provide.

The combustion chamber model [6] simulates the breakup of the jet of LP entering the chamber and the combustion of the resulting droplets. It captures the pressure waves as they move around the chamber, causing pressure oscillations at the chamber end of the orifice. The mass flow rate of the LP into the chamber, however, is computed by the lumped parameter model, and the shape of the velocity profile across the orifice is approximated.

The current work involves the modeling of the liquid reservoir and the orifice in the 30-mm RLPG. The goal of this work is the development of a model that can capture the features of the flow in the orifice. The model used in this work was introduced previously [7]. Because of the complicated shape of the RLPG interior, the use of unstructured meshes and an automatic mesh generator makes discretization of the computational domain much easier. The finite element method was chosen for the model because of its ability to automatically handle unstructured meshes.

Also, the motion of the pistons changes the size and shape of the domain; therefore, the Deformable-Spatial-Domain/Stabilized-Space-Time (DSD/SST) formulation [8–10] of the governing equations is used. In the DSD/SST formulation, a finite element discretization of both space and time is performed. Because of this, the changes in the size and shape of the computational domain can be handled automatically, even if, as in this case, the changes

are not know ahead of time and must be computed as part of the overall solution. The DSD/SST formulation works by treating time as another spatial dimension. The cost is that a two-dimensional spatial problem becomes a three-dimensional space-time problem. To minimize this cost, the space-time domain is subdivided into space-time slabs, analogous to time steps in a semi-discrete formulation. The DSD/SST formulation is then solved one space-time slab at a time.

Two stabilization methods are used in the simulation of the RLPG. The first is the streamline-upwind/Petrov-Galerkin (SUPG) method [11], which controls the instability caused by advection-dominated flows. It has been used in modeling a variety of compressible fluid flow problems [12, 13]. The second stabilization method is a discontinuity capturing method [14], which prevents overshoot and undershoot in the neighborhood of shocks and sharp gradients. It also has been used in a variety of flow problems [13, 15]. While there are no shocks in the interior of the RLPG, there are sharp shear layers between the jet of LP entering the combustion chamber and the rest of the LP in the chamber.

2. Governing Equations

In the numerical model discussed in this paper, the propellant is assumed to be single phase throughout the gun. The propellant, which in the RLPG is XM46, must be assumed to be compressible, because of the high pressure in the gun. It is often convenient to use the bulk modulus to compute the compressibility of a liquid. The bulk modulus is defined as

$$K = \rho \left(\frac{\partial p}{\partial \rho} \right)_{\theta} \tag{1}$$

and is assumed to be a linear function of the pressure, i.e.,

$$K = K_1 + K_2 p. \tag{2}$$

In these equations, K is the bulk modulus and ρ, p, and θ are the density, pressure and temperature of the liquid. Also, K_1 and K_2 are experimentally determined constants. For

any situation in which the pressure of the liquid is within an order of magnitude of the bulk modulus (as is the case in the RLPG), the compressibility of the liquid cannot be neglected.

Equations (1) and (2) can be combined to generate the equation of state for this compressible liquid,

$$p = \frac{K_1}{K_2}\left[\left(\frac{\rho}{\rho_0}\right)^{K_2} - 1\right]. \tag{3}$$

The density at gage pressure of zero is ρ_0. The pressure of the liquid is a function of only density; therefore, the liquid is said to be barotropic.

The dynamics of the liquid in the model are governed by the compressible Navier-Stokes equations. Since the propellant is barotropic, and its viscosity is assumed to be constant, the conservation of energy equation decouples from the conservation of mass and momentum equations. Only the latter are required to describe the flow of the liquid. The former can be solved using data from the other equations, if desired. The conservation of mass and momentum equations can be written in conservation law form as $\forall \mathbf{x} \in \Omega_t, t \in (0,T)$

$$\frac{\partial \rho}{\partial t} + \nabla \cdot (\rho \mathbf{u}) = 0 \tag{4}$$

$$\frac{\partial (\rho \mathbf{u})}{\partial t} + \nabla \cdot (\mathbf{u}\rho\mathbf{u}) + \nabla p = \nabla \cdot \mathbf{T}, \tag{5}$$

where t is time, $(0,T)$ is the time span of interest, and Ω_t is the spatial domain. The subscript "t" implies that the spatial domain may be changing with time. Γ_t is the boundary of Ω_t. Also, $\mathbf{u}$ is the fluid velocity, and $\mathbf{T}$ is the Newtonian viscous stress tensor, defined as

$$\mathbf{T} = \mu\left(\nabla \mathbf{u} + (\nabla \mathbf{u})^T - \frac{2}{3}(\nabla \cdot \mathbf{u})\mathbf{I}\right), \tag{6}$$

where μ is the viscosity of the liquid, and $\mathbf{I}$ is the identity tensor.

The geometry of the RLPG and the flow features of interest are axisymmetric. Assuming axisymmetry of the solution, the governing equations, equations (4) and (5), are written in conservation variables form as $\forall \mathbf{x} \in \Omega_t, t \in (0,T)$

$$\frac{\partial \mathbf{U}}{\partial t} + \frac{\partial \mathbf{F}_z}{\partial z} + \frac{\partial \mathbf{F}_r}{\partial r} + \mathbf{S}_r - \nabla \cdot \mathbf{E} = \mathbf{0}. \tag{7}$$

The radial and axial coordinates are denoted r and z. $\mathbf{U}$, $\mathbf{F}_z$, and $\mathbf{F}_r$ are the vector of conservation variables and the Euler flux vectors, respectively. They are defined as

$$\mathbf{U} = \begin{pmatrix} \rho \\ \rho u_z \\ \rho u_r \end{pmatrix}, \mathbf{F}_z = \begin{pmatrix} u_z \rho \\ u_z \rho u_z + p \\ u_z \rho u_r \end{pmatrix}, \text{ and } \mathbf{F}_r = \begin{pmatrix} u_r \rho \\ u_r \rho u_z \\ u_r \rho u_r + p \end{pmatrix}. \tag{8}$$

Also,

$$\mathbf{S}_r = \frac{u_r}{r}\mathbf{U}. \tag{9}$$

$\mathbf{E}$ contains the dissipative terms and is defined as

$$\mathbf{E} = \begin{pmatrix} \mathbf{0} \\ \mathbf{T} \end{pmatrix}. \tag{10}$$

Equation (7) can be written in quasi-linear form as: $\forall \mathbf{x} \in \Omega_t, t \in (0,T)$

$$\frac{\partial \mathbf{U}}{\partial t} + \mathbf{A}_z \frac{\partial \mathbf{U}}{\partial z} + \mathbf{A}_r \frac{\partial \mathbf{U}}{\partial r} + \mathbf{S}_r - \nabla \cdot \mathbf{E} = \mathbf{0}. \tag{11}$$

$\mathbf{A}_z$ and $\mathbf{A}_r$ are the Jacobians of $\mathbf{F}_z$ and $\mathbf{F}_r$ with respect to $\mathbf{U}$,

$$\mathbf{A}_z = \frac{\partial \mathbf{F}_z}{\partial \mathbf{U}}, \quad \mathbf{A}_r = \frac{\partial \mathbf{F}_r}{\partial \mathbf{U}}. \tag{12}$$

Appropriate boundary and initial conditions are added to equation (11) to complete the problem.

3. Numerical Model

The initial geometry of the RLPG interior is fairly complex. In addition, because the pistons move a large amount during the firing cycle, a new mesh must be generated from time to time during the simulation to prevent excessive mesh distortion. For these reasons, an automatic mesh generator, which uses Delaunay-Voronoï methods [16], is used to discretize the spatial domain using an unstructured mesh, which consists of three-node triangular elements. These triangular elements in space are made into six-node prism elements in the space-time domain by adding the temporal dimension to each element.

The space-time domain is subdivided into space-time slabs by partitioning the temporal dimension $(0, T)$ into subintervals $I_n = (t_n, t_{n+1})$, where $0 = t_0 < t_1 < \cdots < t_N = T$. The time slab corresponding to I_n (denoted Q_n) is enclosed by Ω_n, Ω_{n+1}, and P_n (where $\Omega_n = \Omega_{t_n}$, and P_n is the surface defined by Γ_t as t varies from t_n to t_{n+1}). Also, P_n is decomposed into $(P_n)_{\mathrm{G}}$ and $(P_n)_{\mathrm{H}}$, the parts of the boundary on which are imposed Dirichlet-type and Neuman-type boundary conditions, respectively.

The function spaces for the trial solutions and the weighting functions, $\mathcal{S}_n^h$ and $\mathcal{V}_n^h$, are defined on each space-time slab. The functions are piecewise linear and continuous in space and piecewise linear in time, but discontinuous across the interface between neighboring space-time slabs. The discontinuity of the shape functions in time means that the mesh used in one space-time slab need not be used in the next slab (i.e., remeshing can occur across the slab interface).

The DSD/SST formulation of equation (11) is, given $(\mathbf{U}^h)_n^-$, find $\mathbf{U}^h \in \mathcal{S}_n^h$, such that $\forall \mathbf{W}^h \in \mathcal{V}_n^h$:

$$\begin{aligned}
&\int_{Q_n} \mathbf{W}^h \cdot \left(\frac{\partial \mathbf{U}^h}{\partial t} + \mathbf{A}_z^h \frac{\partial \mathbf{U}^h}{\partial z} + \mathbf{A}_r^h \frac{\partial \mathbf{U}^h}{\partial r} + \mathbf{S}_r^h \right) dQ \\
&\quad + \int_{Q_n} \nabla \mathbf{W}^h : \mathbf{E}^h dQ \quad + \quad \int_{\Omega_n} (\mathbf{W}^h)_n^+ \cdot ((\mathbf{U}^h)_n^+ - (\mathbf{U}^h)_n^-) \, d\Omega \\
&+ \sum_{e=1}^{(n_{el})_n} \int_{Q_n^e} \boldsymbol{\tau} \left((\mathbf{A}_z^h)^T \frac{\partial \mathbf{W}^h}{\partial z} + (\mathbf{A}_r^h)^T \frac{\partial \mathbf{W}^h}{\partial r} \right) \cdot \left(\frac{\partial \mathbf{U}^h}{\partial t} + \mathbf{A}_z^h \frac{\partial \mathbf{U}^h}{\partial z} + \mathbf{A}_r^h \frac{\partial \mathbf{U}^h}{\partial r} + \mathbf{S}_r^h \right) dQ \\
&\quad + \sum_{e=1}^{(n_{el})_n} \int_{Q_n^e} \delta \left(\frac{\partial \mathbf{W}^h}{\partial z} \cdot \frac{\partial \mathbf{U}^h}{\partial z} + \frac{\partial \mathbf{W}^h}{\partial r} \cdot \frac{\partial \mathbf{U}^h}{\partial r} \right) dQ \quad = \quad \int_{(P_n)_{\mathbf{H}}} \mathbf{W}^h \cdot \mathbf{H}^h \, dP. \qquad (13)
\end{aligned}$$

In this formulation,

$$(\mathbf{U}^h)_n^{\pm} = \lim_{\epsilon \to 0} \mathbf{U}(t_n \pm \epsilon), \qquad (14)$$

$$\int_{Q_n} (\ldots) dQ = \int_{I_n} \int_{\Omega_n} (\ldots) \, d\Omega \, dt, \qquad (15)$$

$$\int_{P_n} (\ldots) dP = \int_{I_n} \int_{\Gamma_n} (\ldots) \, d\Gamma \, dt. \qquad (16)$$

Equation (13) is applied sequentially to $Q_0, Q_1, \ldots, Q_{N-1}$, with

$$(\mathbf{U}^h)_0^- = \mathbf{U}_0^h, \qquad (17)$$

where $\mathbf{U}_0$ is the initial value of $\mathbf{U}$.

The time-discontinuous Galerkin formulation of equation (11) consists of the first three terms on the left-hand side and the term on the right of equation (13). The third term on the left weakly enforces continuity of the solution across slab interfaces. The SUPG term is the fourth term on the left, consisting of a series of element level integrals. The discontinuity capturing term is the fifth term on the left.

The discontinuity capturing coefficient, δ, is [17]

$$\delta = \left[\frac{\| \mathbf{A}_z^h \frac{\partial \mathbf{U}^h}{\partial z} + \mathbf{A}_r^h \frac{\partial \mathbf{U}^h}{\partial r} + \mathbf{S}_r^h \|^2_{\widetilde{\mathbf{A}}_0^{-1}}}{\sum_{j=1}^{n_{sd}} \left(\| \frac{\partial \xi_j}{\partial x_z} \frac{\partial \mathbf{U}}{\partial x_z} \|^2_{\widetilde{\mathbf{A}}_0^{-1}} + \| \frac{\partial \xi_j}{\partial x_r} \frac{\partial \mathbf{U}}{\partial x_r} \|^2_{\widetilde{\mathbf{A}}_0^{-1}} \right)} \right]^{\frac{1}{2}}. \tag{18}$$

The SUPG coefficient, $\boldsymbol{\tau}$, is a diagonal matrix defined as [10]

$$\boldsymbol{\tau} = \max[\mathbf{0}, \boldsymbol{\tau}_a - \boldsymbol{\tau}_\delta - \boldsymbol{\tau}_d]. \tag{19}$$

The contribution from the advection terms is $\boldsymbol{\tau}_a$; $\boldsymbol{\tau}_\delta$ and $\boldsymbol{\tau}_d$ are corrections for the discontinuity capturing term and the physical diffusion. Without the correction terms, the solution is overly diffuse. The terms in equation (19) are defined as

$$\boldsymbol{\tau}_a = \frac{h \max(|\beta_i|)}{2(c + |\mathbf{u} \cdot \beta|)} \mathbf{I}, \tag{20}$$

$$\boldsymbol{\tau}_\delta = \frac{\delta}{(c + |\mathbf{u} \cdot \beta|)^2} \mathbf{I}, \tag{21}$$

$$\boldsymbol{\tau}_d = \frac{\beta_1^2 \mathbf{K}_z + \beta_2^2 \mathbf{K}_r}{(c + |\mathbf{u} \cdot \beta|)^2}. \tag{22}$$

The element length and the speed of sound in the fluid are denoted h and c. Also,

$$\beta = \frac{\nabla \| \mathbf{U} \|_2^2}{\| \nabla \| \mathbf{U} \|_2^2 \|_2} \tag{23}$$

and

$$\mathbf{K}_z = \begin{pmatrix} 0 & 0 & 0 \\ 0 & \frac{4}{3}\mu & 0 \\ 0 & 0 & \mu \end{pmatrix} \text{ and } \mathbf{K}_r = \begin{pmatrix} 0 & 0 & 0 \\ 0 & \mu & 0 \\ 0 & 0 & \frac{4}{3}\mu \end{pmatrix}. \tag{24}$$

In equation (13),

$$\begin{aligned}\nabla \mathbf{W}^h : \mathbf{E}^h &= 2\mu \frac{\partial w_r}{\partial r}\frac{\partial u_r}{\partial r} - \frac{2}{3}\mu \frac{\partial w_r}{\partial r}(\nabla \cdot \mathbf{u}) \\ &+\mu \left(\frac{\partial w_z}{\partial r} + \frac{\partial w_r}{\partial z}\right)\left(\frac{\partial u_z}{\partial r} + \frac{\partial u_r}{\partial z}\right) \\ &+2\mu \frac{\partial w_z}{\partial z}\frac{\partial u_z}{\partial z} - \frac{2}{3}\mu \frac{\partial w_z}{\partial z}(\nabla \cdot \mathbf{u}) \\ &+2\mu \frac{w_r}{r}\frac{u_r}{r} - \frac{2}{3}\mu \frac{w_r}{r}(\nabla \cdot \mathbf{u}),\end{aligned} \tag{25}$$

where

$$\nabla \cdot \mathbf{u} = \frac{\partial u_z}{\partial z} + \frac{\partial u_r}{\partial r} + \frac{u_r}{r}, \tag{26}$$

and w_z and w_r denote the weighting functions corresponding to the axial and radial momentum balance equations.

During the simulation of the firing cycle, the mesh moves, based on the motion of the pistons. An automatic mesh-moving scheme [18] treats the computational domain as an elastic solid. The motion of the pistons is used as input for the mesh-moving scheme, which then computes the new location of the interior nodes. In order to prevent excessive distortion of the mesh, a new mesh is generated periodically using the automatic mesh generator.

Equation (13) generates a system of coupled nonlinear equations in each time slab. The equation system is solved using the Newton-Raphson method. The Generalized Minimal Residual (GMRES) algorithm [19], with a diagonal preconditioner, is used to solve the linear equation system generated by the Newton-Raphson method.

When the code enters a space-time slab, the flow variables in the new space-time slab are set equal to the flow variables in the previous slab. The motion of the injection piston is estimated using the fluid data from the previous time slab, and the mesh is updated, based

on the piston motion. The fluid simulation is updated using the new mesh and piston motion. A second iteration is performed between the piston motion, the mesh, and the flow variables. In general, two iterations between the three parts of the code within each space-time slab provide sufficient convergence.

4. Model of LP Flow in the 30-mm RLPG

The DSD/SST formulation (equation (13)) was used to model the flow of the LP during test firings of the 30-mm RLPG. At the beginning of the firing cycle, the pistons are in contact, separating the reservoir from the combustion chamber. The ability to handle the merging of two computational domains into one as a part of the simulation has not been added to this model. Therefore, the pistons are slightly separated at the beginning of the simulation. The opening is so small, however, that only one element spans the gap. Since there are no-slip boundary conditions on the piston surfaces, no LP can flow through the orifice, as though the pistons were in contact. This approximation has worked quite well.

As mentioned previously, the LP is assumed to be a single phase throughout the LP interior; no combustion is included in the current model. Since the combustion chamber in the actual gun is primarily filled with gas resulting from combustion, the current model does not properly simulate the flow in the chamber. Therefore, while the computational domain includes the entire liquid reservoir and orifice, it does not include the entire combustion chamber (see Figure 2). The boundary that cuts the combustion chamber moves with the pistons during the firing cycle. To include the effect of combustion in the simulation, the pressure in the combustion chamber is taken from experimental data or a lumped parameter simulation of the shot and imposed on the boundary of the computational domain in combustion chamber.

The motion of the injection (outer) piston is computed, based on the pressure forces from the LP acting on it. Viscous and friction forces on this piston are neglected. The injection piston is not allowed to overtake the control piston. The damper, which sits behind the control piston, is not modeled. To include the effect of the damper, the motion of the

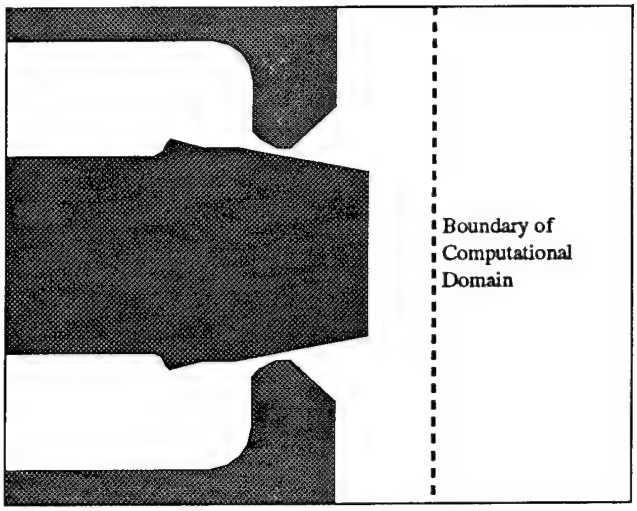

Figure 2. The Computational Domain Used in This Study.

control piston is taken from experimental data or a lumped parameter simulations of the shot. Both of the pistons act as rigid bodies and only move axially.

The model of the RLPG assumes axisymmetry. A no-slip boundary condition is imposed on the solid surfaces, and a no-penetration boundary condition is imposed on the symmetry axis. The reservoir is initially prepressurized, while the chamber is initially at ambient pressure. The initial condition of the pressure in the simulation reflects the prepressurization. The initial pressure varies linearly along the length of the orifice to prevent a stability problem caused by having a jump in the initial pressure at one point.

5. 30-mm RLPG Test Firings

The 30-mm RLPG was fired at the U.S. Army Research Laboratory at Aberdeen Proving Ground, MD. The LP used was XM46, a monopropellant composed of hydroxyl ammonium nitrate (HAN), triethanol ammonium nitrate (TEAN) and water. The constants in equation (3) for XM46 are $K_1 = 5350$ MPa, $K_2 = 9.11$, and $\rho_0 = 1430 \frac{\text{kg}}{\text{m}^3}$. Two shots of the 30-mm RLPG were simulated: shots 38 and 128.

5.1 Shot 38. Shot 38 was fired using 94.3 cm^3 of LP and an initial chamber volume of 290 cm^3 [20]. While the chamber and reservoir pressure data from this shot are considered

to be accurate, the piston travel data are suspect. Therefore, the data used as input for this simulation came from a lumped parameter model of the shot, which agreed quite well with the experimental pressure. The mesh of the initial computational domain and a closeup of the mesh in the orifice are shown in Figure 3. The initial mesh consists of 3,029 spatial nodes and 5,557 elements. As the firing cycle proceeds and the pistons move, a new mesh is periodically generated. In this simulation, a new mesh was generated every 10 time steps (the time step size was 0.0167 ms) until 12.6 ms, when a new mesh was generated every time step because the injection piston and the back wall of the reservoir were so close together.

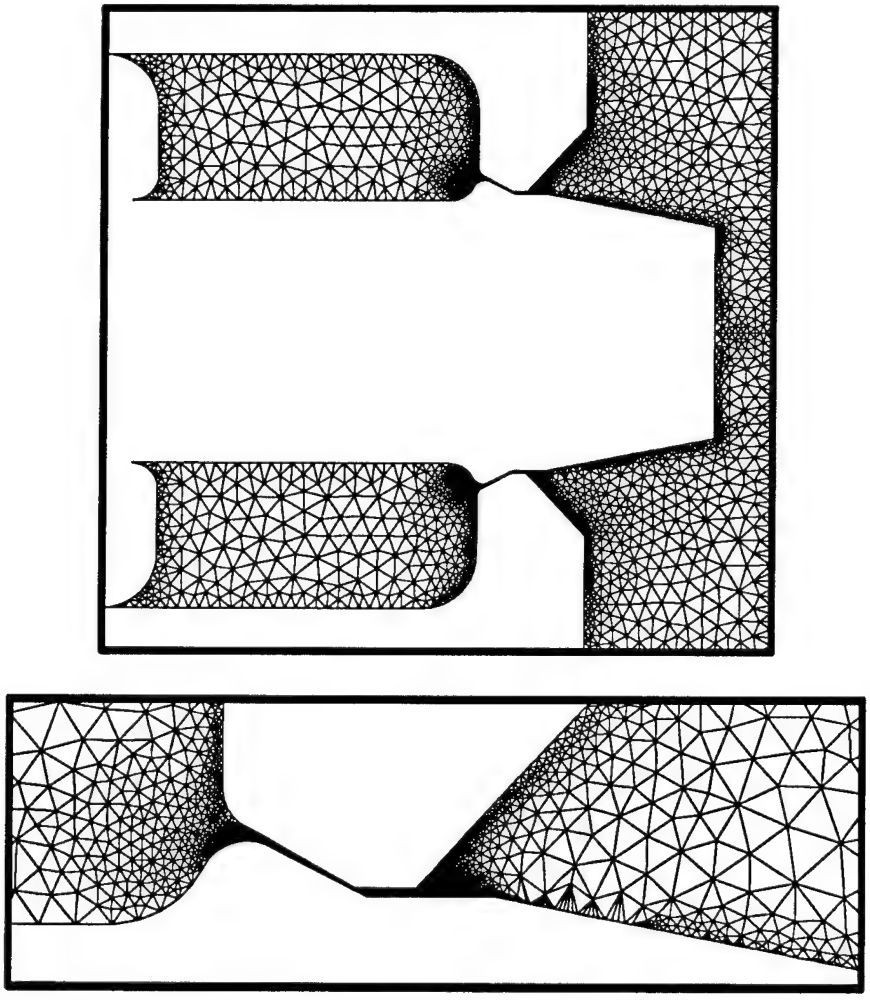

Figure 3. Shot 38: Mesh at Time 4.4 ms.

Time t = 0 was set to be the beginning of the ignition sequence, which lasted until 4.4 ms. The simulation started once the ignition sequence ended, and, in keeping with the timing of the experiment, the initial time of the simulation was set to 4.4 ms. The meshes at times 6.4 ms, 8.4 ms, 10.4 ms, and 12.4 ms are shown in Figures 4 and 5. The meshes in the orifice are shown in Figure 6. The meshes used during the simulation of shot 38 ranged in size from 5,600-14,500 elements and 3,000-7,500 spatial nodes. The meshes shown in Figures 4 and 5 have 5,176, 5,445, 5,575, and 4,526 spatial nodes and 9,851, 10,389, 10,649, and 8,591 elements, respectively.

The computational domain is noticeably larger at 8.4 ms than at 10.4 ms, as can be seen in Figures 4 and 5, but the meshes have roughly the same number of nodes and elements. As can be seen in Figure 6, the orifice at both times is nearly the same size. Since the majority of the nodes and elements are in the orifice, there are about as many nodes and elements at 8.4 ms as at 10.4 ms.

Control piston motion and chamber pressure data from a lumped parameter simulation of shot 38 were used as input for the DSD/SST simulation. In the test firing, the reservoir pressure was measured in the middle of the back wall of the reservoir. Therefore, the pressure predicted by the model for the middle of the back wall of the reservoir is recorded and compared to the lumped parameter data, which agree well with the experimental data. The reservoir pressure from experimental data, the current model, and the lumped parameter model, and the chamber pressure from the experimental data and the lumped parameter model are shown in Figure 7.

The agreement between the results of the DSD/SST model and the lumped parameter model is good, and both models agree quite well with the experiment. The oscillations early in the firing cycle are caused by the piston and the column of fluid in the reservoir acting as a mass and spring. The oscillations in the data from the DSD/SST model late in the firing cycle are caused by remeshing. This is corrected in the later simulations by using a smaller time step. A time step size of 0.01 ms is sufficient, resulting in a new mesh being generated every 0.1 ms, instead of every 0.167 ms.

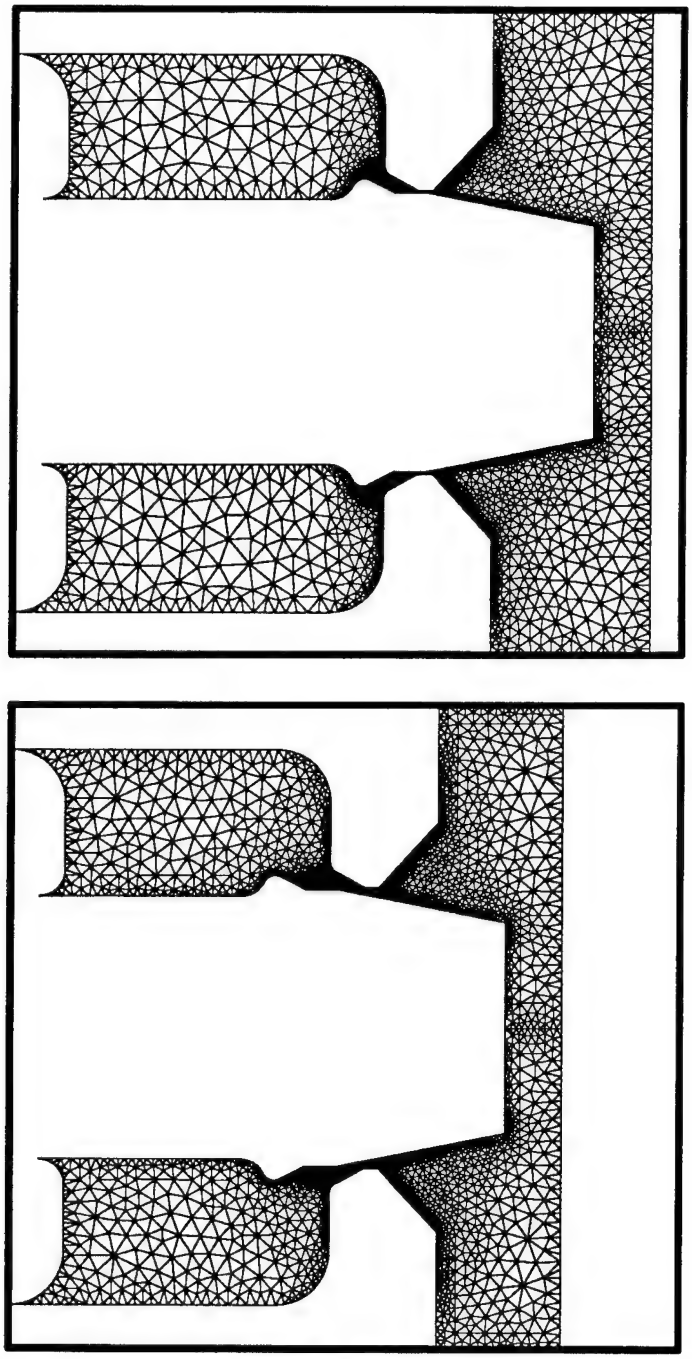

Figure 4. Shot 38: Global View of Mesh at Times 6.4 ms and 8.4 ms.

The injection piston motion from the DSD/SST and the lumped parameter simulations of shot 38 and the experimental data and the control piston motion from the lumped parameter simulation and the experimental data are shown in Figure 8. The predicted piston travels

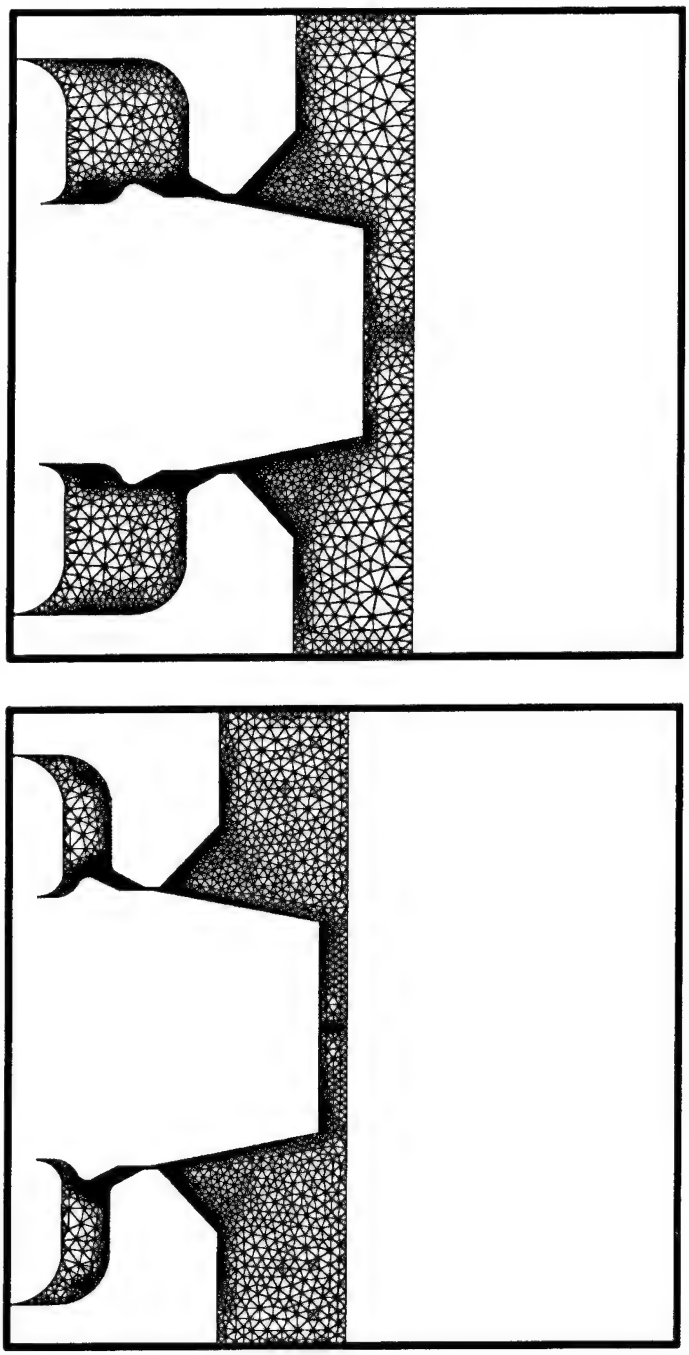

Figure 5. Shot 38: Global View of Mesh at Times 10.4 ms and 12.4 ms.

do not agree well with the experimental data. The injection piston motion data from the numerical models agree reasonably well, although some differences are seen. The lumped parameter model assumes that flow through the orifice is developed immediately, while in the

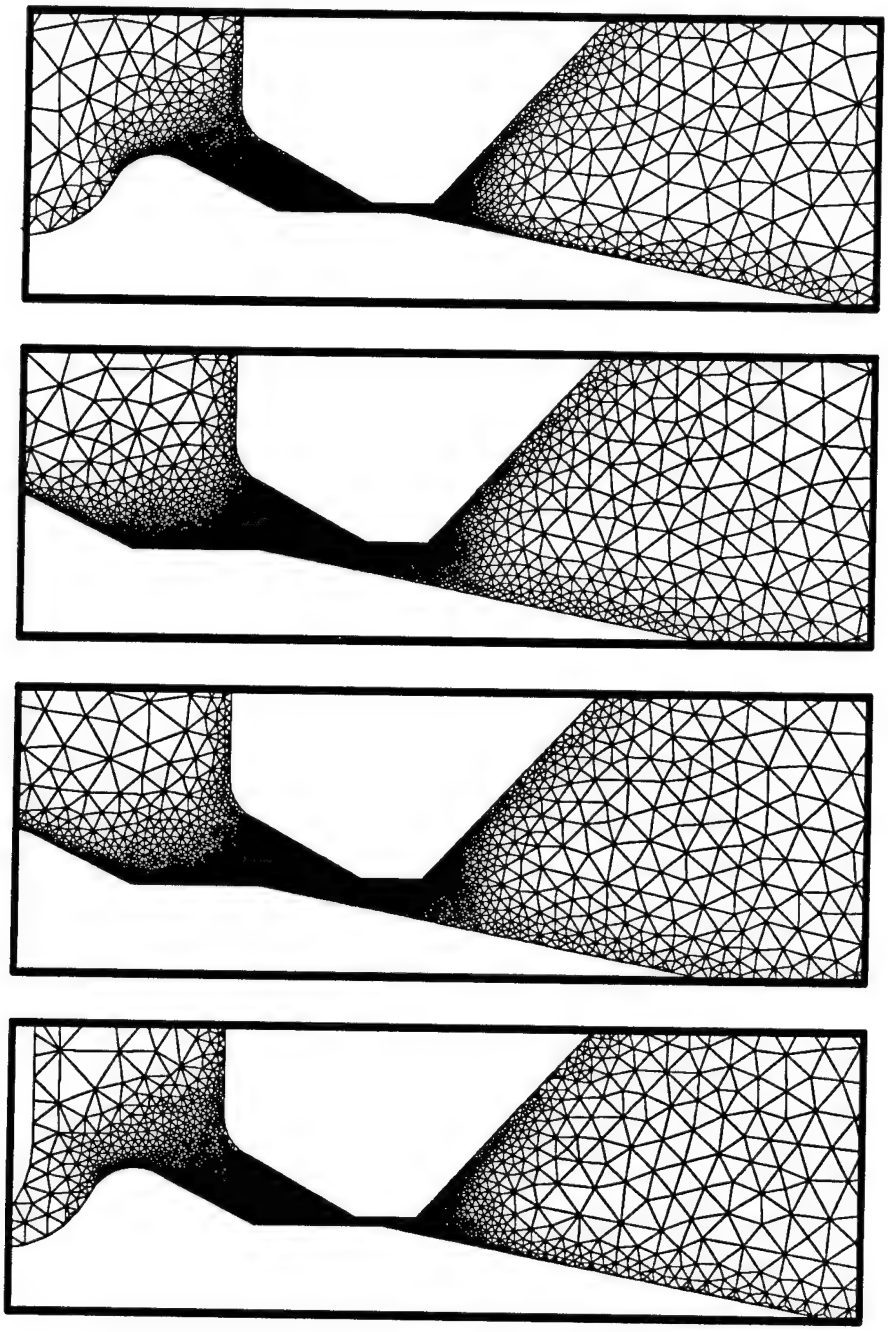

Figure 6. Shot 38: Mesh in the Orifice at Times 6.4 ms, 8.4 ms, 10.4 ms, and 12.4 ms.

DSD/SST model, the flow needs time to develop. This causes the early difference in injection piston travel seen in Figure 8; in the DSD/SST model, the injection piston is slowed while flow in the orifice develops. Later in the firing cycle, the injection piston in the DSD/SST model nearly catches up with the injection piston in the lumped parameter simulation.

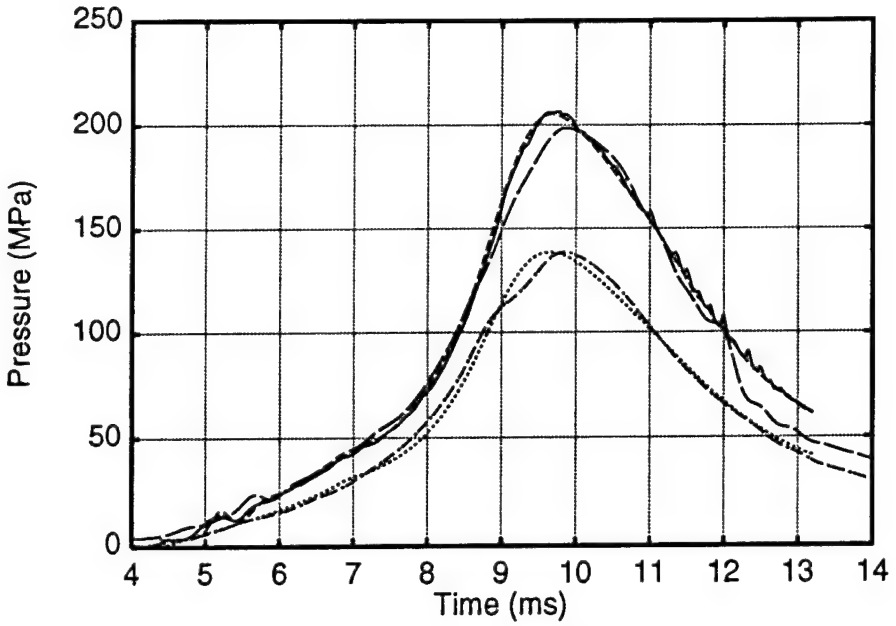

Figure 7. Shot 38: Pressure at the Back Wall of the Reservoir: DSD/SST Prediction (Line), Lumped Parameter Model (Dash), and Experimental Data (Long Dash). Pressure in the Combustion Chamber: Lumped Parameter Model (Dot) and Experimental Data (Dot-Dash).

The last test of the accuracy of the DSD/SST model is the discharge coefficient of the orifice, defined as

$$c_D = \frac{m_f}{A\sqrt{2\rho_r\left(p_r - p_c\right)}}. \tag{27}$$

The mass flow rate of the LP through the orifice is denoted m_f; p_r, p_c, and ρ_r are the pressure in the reservoir and the chamber and the density in the reservoir, respectively. A is the cross-sectional area of the orifice. The generally accepted value for the discharge coefficient is 0.95 [1]. The discharge coefficient is computed by the DSD/SST model and is shown in Figure 9. During the first 2 ms of the simulation, the flow is developing and the discharge coefficient rises rapidly. It levels off between 0.85 and 0.9, which is a little lower than expected. This means that the mass flow rate of LP per unit area through the orifice computed by the model is likely a little lower than what actually occured in shot 38.

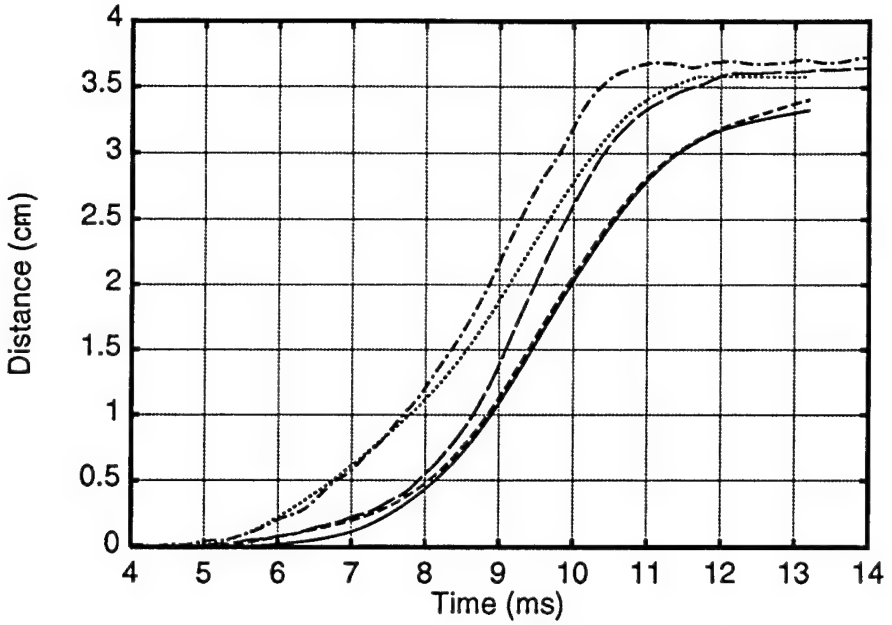

Figure 8. Shot 38: Motion of the Injection Piston: DSD/SST Prediction (Line), Lumped Parameter Model (Dash), and Experiment (Long Dash). Motion of the Control Piston: Lumped Parameter Model (Dot) and Experiment (Dot-Dash).

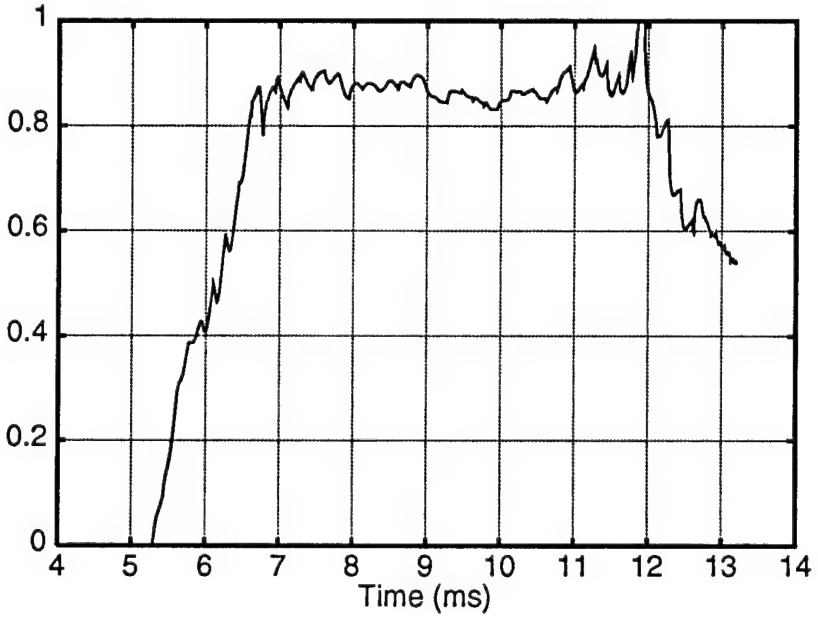

Figure 9. Shot 38: Discharge Coefficient in the Orifice: DSD/SST Prediction.

The low discharge coefficient means that the model is predicting more kinetic energy loss in the orifice than occurs in the physical gun. The method of the kinetic energy loss is

probably its conversion to heat by viscous effects. In the model used in this work, the drivers of the problem are the motion of the control piston and the pressure rise in the chamber. For this shot, these values were input to the model, coming from the lumped parameter model with its discharge coefficient of 0.95. The only effect of the low discharge coefficient in the model is that the cross-sectional area of the orifice is a little larger in the model than in the lumped parameter model. This is seen in Figure 8, in that the injection piston motion computed by the DSD/SST model never catches up with that computed by the lumped parameter model.

Since the reservoir pressure, the injection piston motion, and the discharge coefficient computed by the DSD/SST model of the RLPG all compare reasonably well with the expected results, the rest of the data generated by this model are considered reasonably accurate. The goal of this project is an understanding of the flow phenomena that occur in the injector region of the RLPG. Figures 10 and 11 show the Mach number distribution of the flow at 6.4 ms, 8.4 ms, 10.4 ms, and 12.4 ms. By 6.4 ms, the orifice has not opened very much, and there is little flow through the orifice. By 8.4 ms, the flow through the orifice is well established, and a recirculation region has developed on the chamber side of the injection piston. The jet of LP entering the combustion chamber still tends to lift off of the nose of the control piston. By 10.4 ms, the flow through the orifice has attained sufficient speed that the jet of LP entering the chamber better follows the control piston, although the jet still has detached by the end of the piston. The recirculation region by the injection piston has grown in strength. At 12.4 ms, the orifice is closing, and the flow of LP into the chamber has almost stopped.

The jet of LP lifts away from the surface of the inner piston at all four times shown in Figures 10 and 11. The point at which the jet leaves the surface varies during the firing cycle, but much of the nose of the control piston is in contact with combustion gases throughout the firing cycle.

Figure 12 show the Mach number distribution in the orifice at the times previously mentioned. The highest Mach number is seen in the throat of the orifice, as expected. The

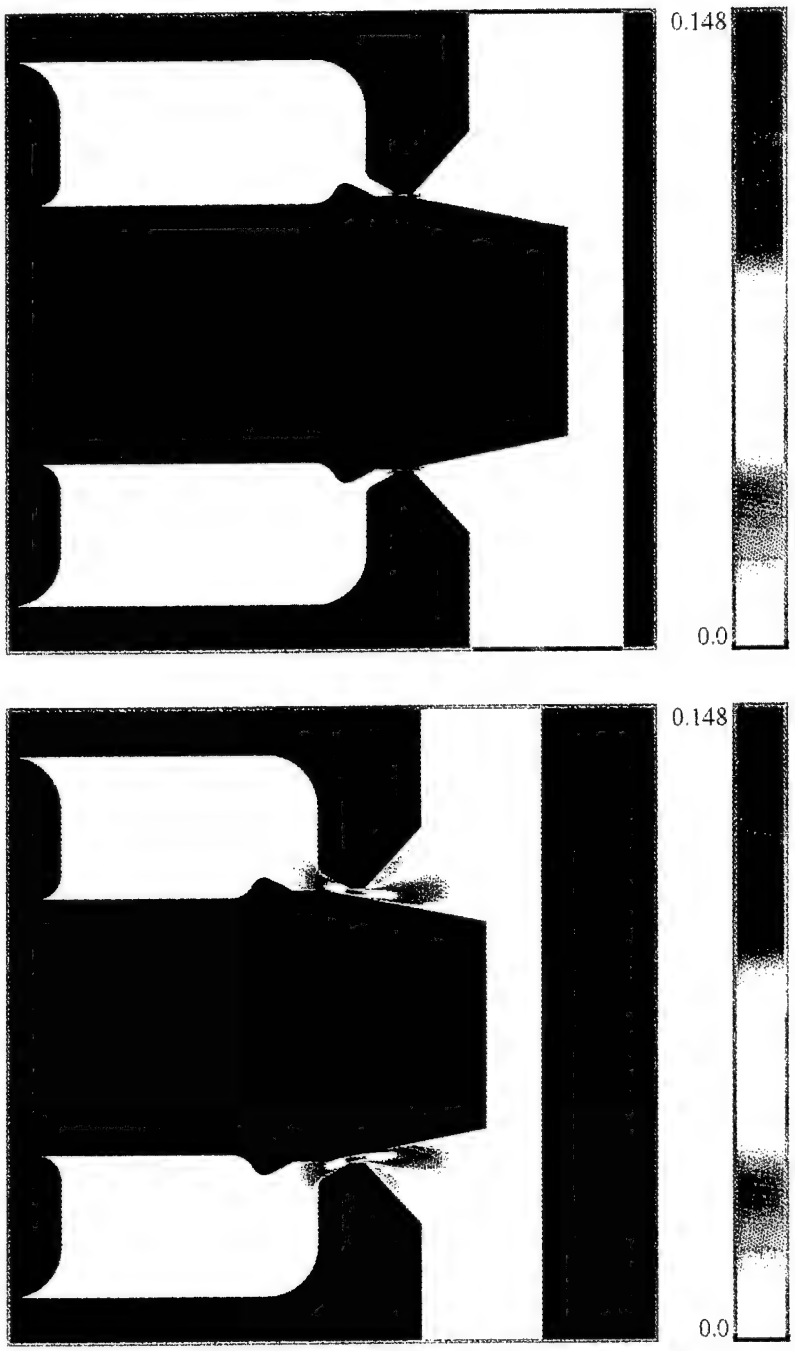

Figure 10. Shot 38: Global View of Mach Number Contours at Times 6.4 ms and 8.4 ms.

recirculation region near the injection piston can be clearly seen. There is no tendency for the flow to separate from the pistons or reverse direction of travel in the orifice. Either of

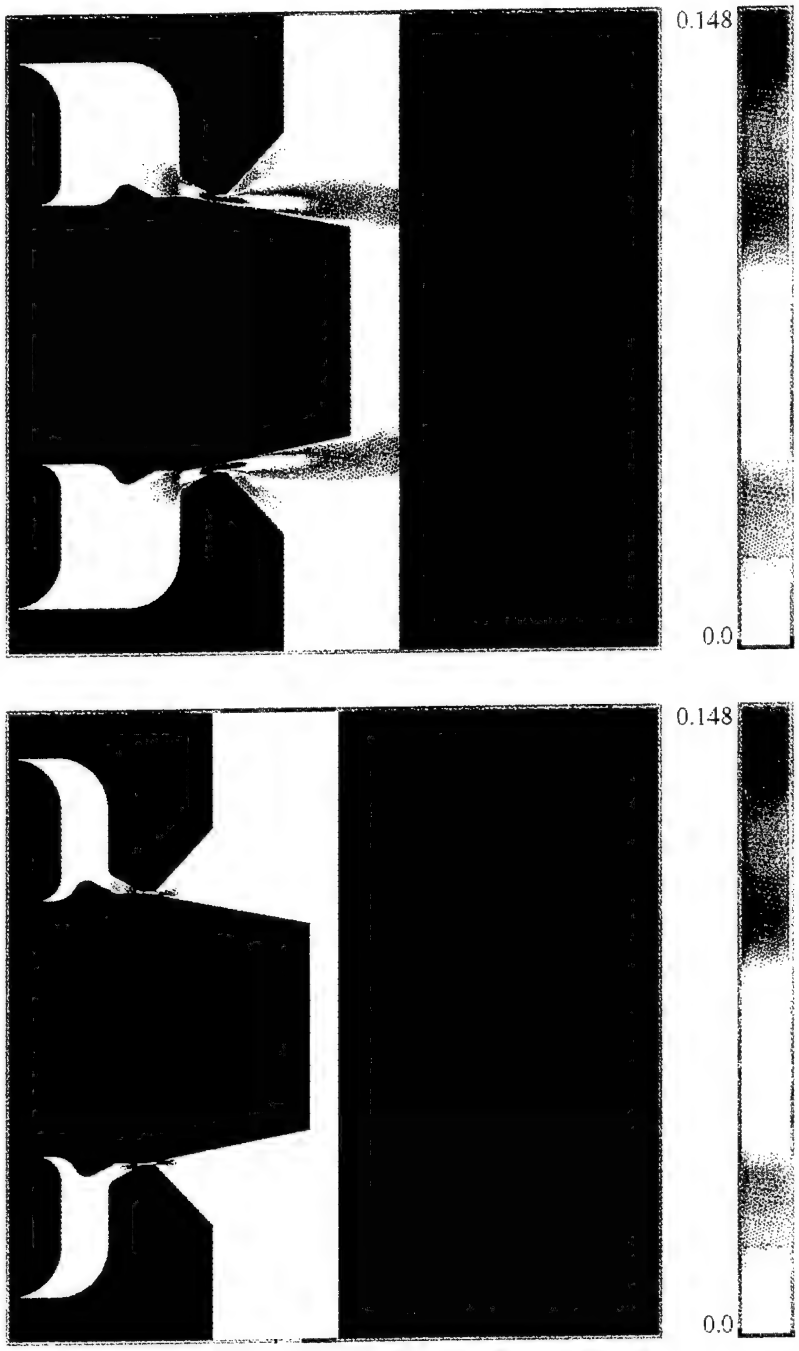

Figure 11. Shot 38: Global View of Mach Number Contours at Times 10.4 ms and 12.4 ms.

these could result in disruption of LP flow in the orifice and possibly cause reversals in the gun.

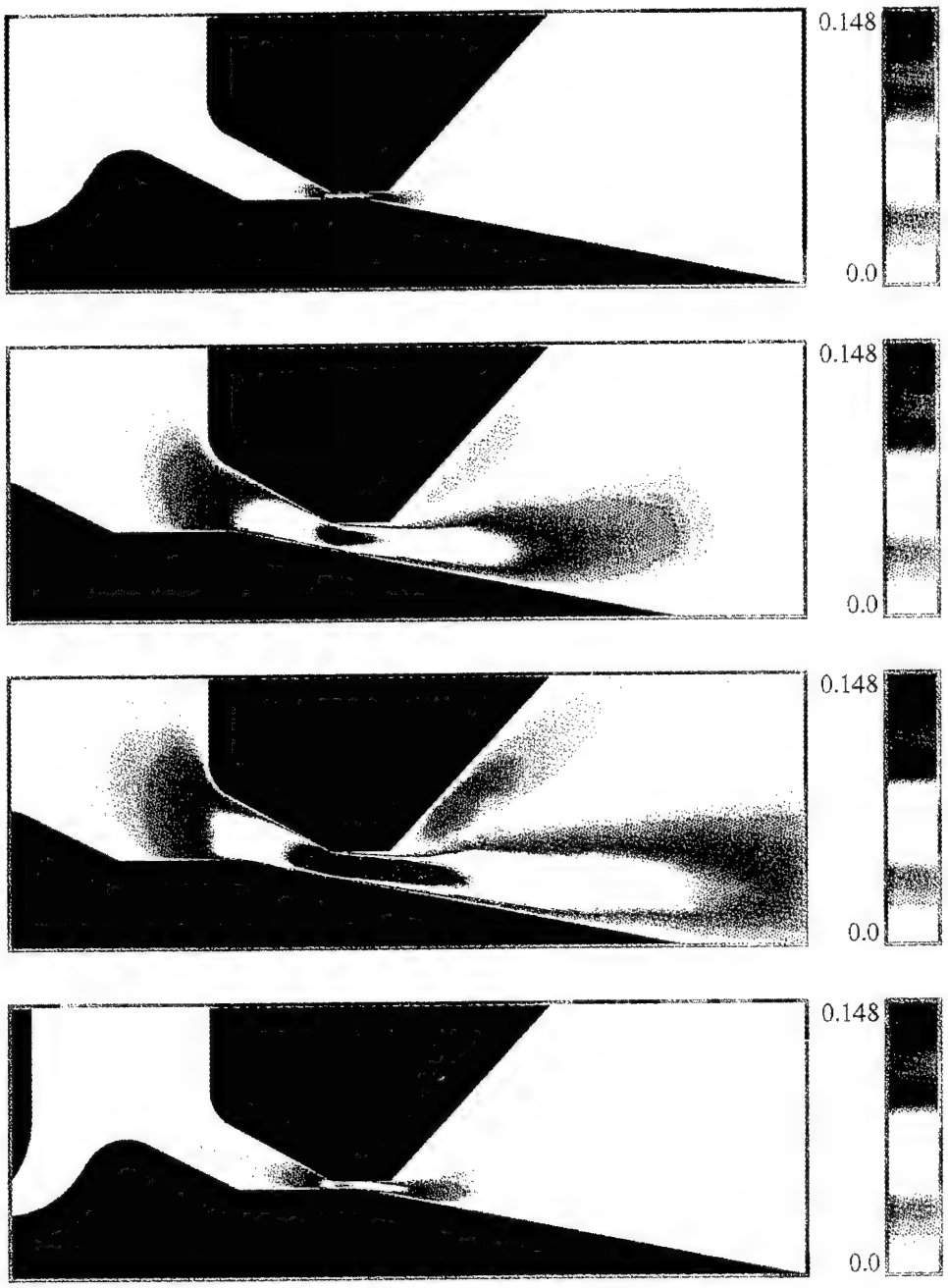

Figure 12. Shot 38: Mach Number Contours in the Orifice at Times 6.4 ms, 8.4 ms, 10.4 ms, and 12.4 ms.

5.2 Shot 128. Shot 128 was fired using 224.1 cm^3 of LP and an initial chamber volume of 290 cm^3 [20]. The ignition sequence started at time t = 0.0. The simulation, which does not include the ignition sequence, started at 5.65 ms. Remeshing was performed every 10

time steps during this simulation. Figures 13 and 14 show the mesh at 10.0 ms, 12.0 ms, 14.0 ms, and 16.0 ms. The meshes have 5,602, 5,449, 8,119, and 7,074 nodes and 10,663, 10,357, 15,697, and 13,655 elements, respectively. As the firing cycle proceeds, the liquid reservoir gets smaller in volume. In the remeshing procedure used in the code, the number of nodes along each wall of the reservoir stays the same; this number can only be changed manually when the code is restarted. As the reservoir decreases in volume, the nodes along two of the boundaries get closer together. Since the mesh in the interior of the reservoir is based on the nodes on the boundary, at 14.0 ms, the mesh in the reservoir is finer than it needs to be. The remeshing procedure should be improved to prevent this.

Figure 15 shows the mesh in the orifice at the times previously mentioned. The mesh, especially along the injection piston, is sufficiently fine to model accurately the flow in the orifice. Notice that the orifice opens noticeably more than in shot 38. This occurs because more than twice the amount of LP has to be injected into the combustion chamber.

Filtered experimental data was used as the input for the control piston motion and the chamber pressure. The computed pressure at the center of the rear wall of the reservoir is plotted with the filtered experimental chamber pressure in Figure 16. The reservoir pressure gauge failed during this shot. Comparing Figure 16 to Figure 7, the computed pressure for shot 128 looks reasonable. The reservoir pressure oscillations near peak pressure are caused by a deceleration of the control piston, and the later oscillations are caused by remeshing.

The ratio between the reservoir pressure and the chamber pressure is approximately equal to the ratio between the surface area on the chamber side and reservoir side of the injection piston, which is 1.47. Early in the firing cycle, as the injection piston is accelerating, the pressure ratio should be a little lower; later, when the piston is decelerating, the ratio should be a little higher. An analysis of the data shown in Figure 16 verifies that this is the case.

The control piston motion measured during shot 128 is shown with the computed injection piston motion in Figure 17. The experimental injection piston motion data from this shot

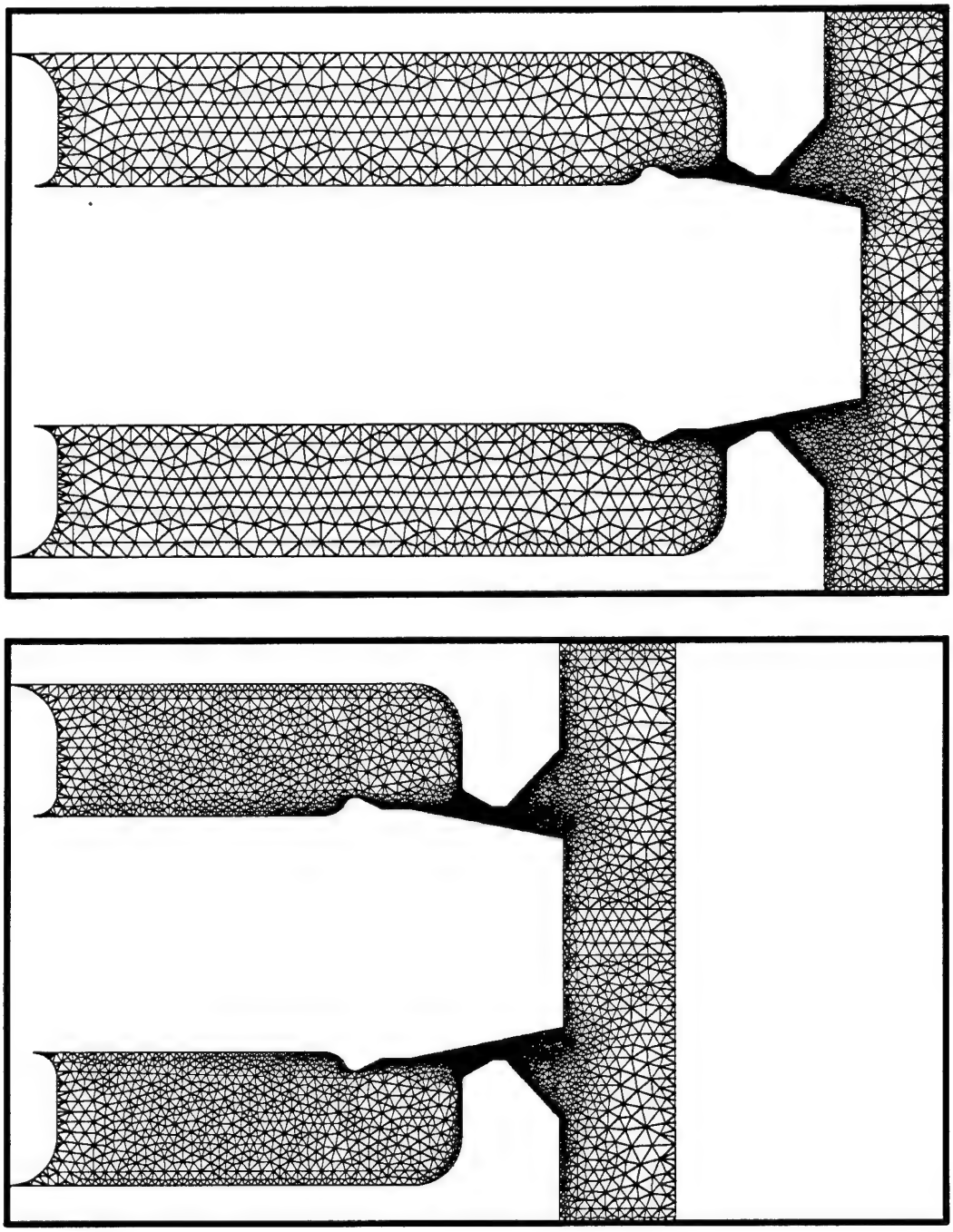

Figure 13. Shot 128: Global View of Mesh at Times 10.0 ms and 12.0 ms.

were not reliable. When compared with Figure 8, the injection piston motion from the simulation of shot 128 is quite reasonable.

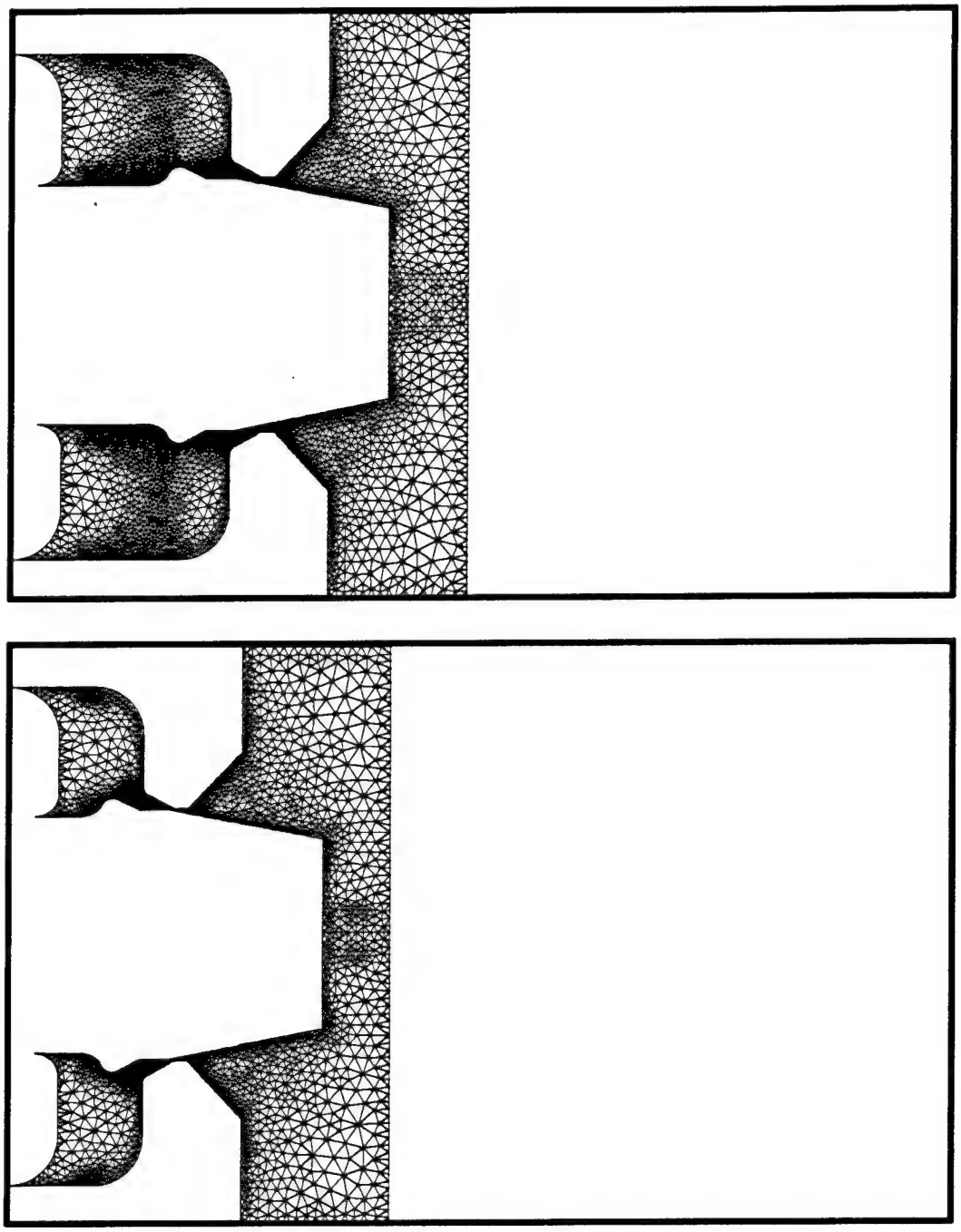

Figure 14. Shot 128: Global View of Mesh at Times 14.0 ms and 16.0 ms.

The discharge coefficient computed during the simulation of shot 128 is shown in Figure 18. The flow in the orifice is fully developed by 8.2 ms. The discharge coefficient drops below zero for a short period of time at the beginning of the simulation. As the injection and

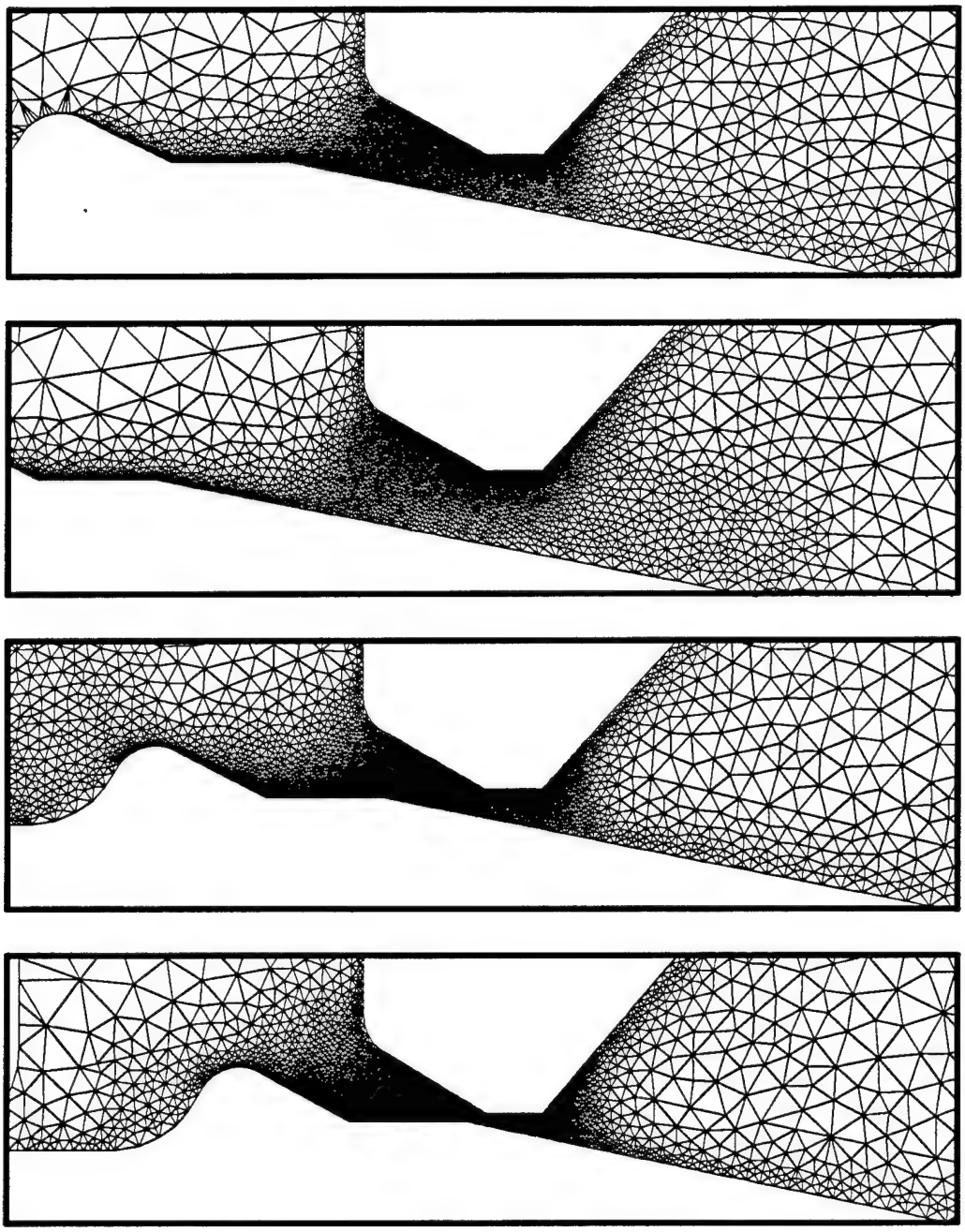

Figure 15. Shot 128: Mesh in the Orifice at Times 10.0 ms, 12.0 ms, 14.0 ms, and 16.0 ms.

control pistons separate, there is a low-pressure region at the center of the orifice, and fluid from both the reservoir and the chamber is drawn into the orifice. As the LP flow develops, the flow from the chamber into the orifice ends quickly. The discharge coefficient in this shot

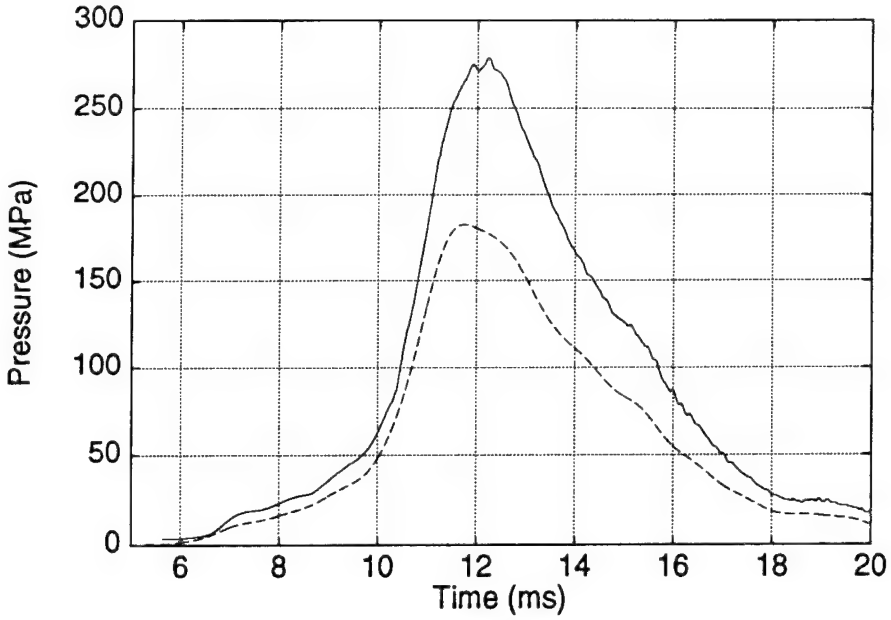

Figure 16. Shot 128: DSD/SST Prediction of Pressure at the Back Wall of the Reservoir (Line). Experimental Pressure in the Combustion Chamber (Dash).

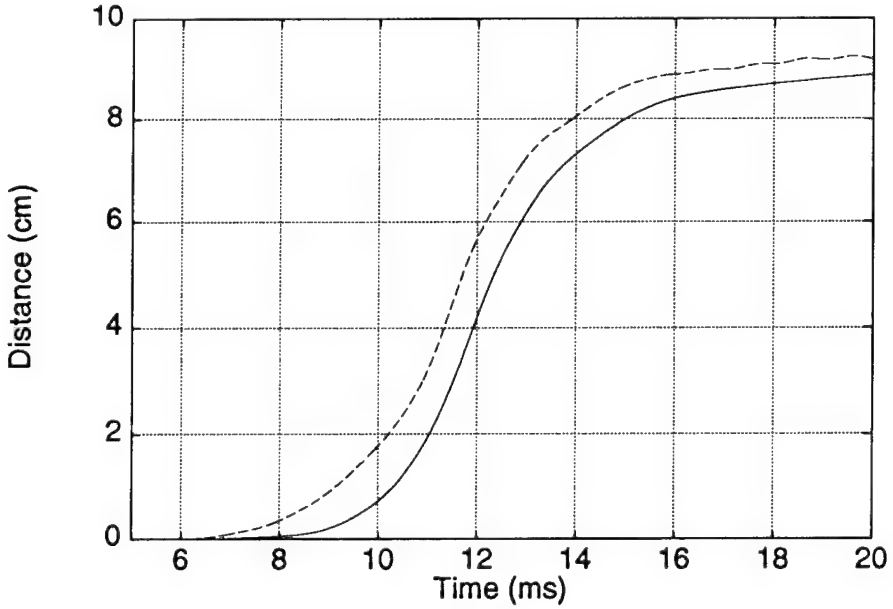

Figure 17. Shot 128: DSD/SST Prediction of Motion of the Injection Piston (Line). Experimental Motion of the Control Piston (Dash).

is once again lower than expected, oscillating between 0.8 and 0.85 vs. the expected value of 0.95. The discharge coefficient is increasing toward the end of the firing cycle.

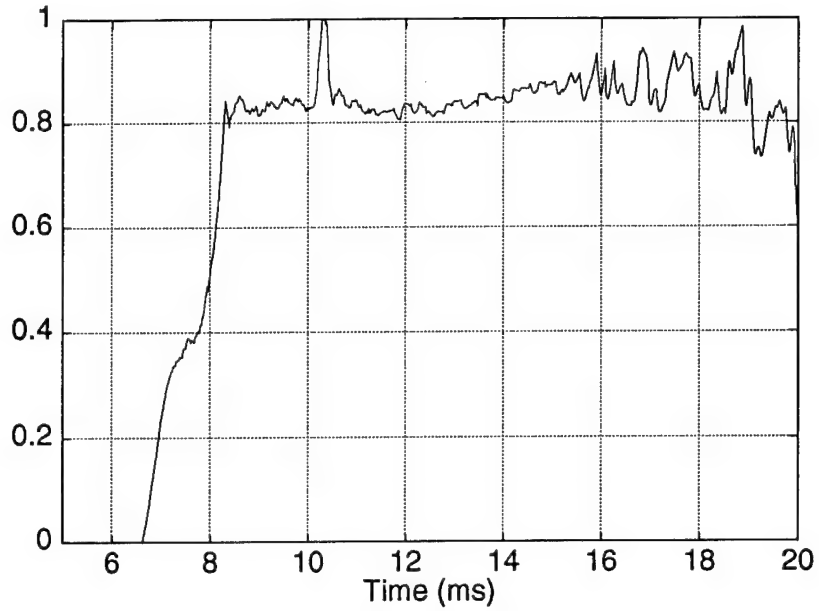

Figure 18. Shot 128: Discharge Coefficient in the Orifice: DSD/SST Prediction.

Figures 19 and 20 show the Mach number at 10.0 ms, 12.0 ms, 14.0 ms, and 16.0 ms. The increased opening between the piston can be seen. This leads to a thicker jet of LP entering the chamber. The jet stays attached to the control piston nose until the end at 12.0 ms and 14.0 ms. This creates a recirculation region at the end of the control piston. At the two other times, the jet lifts off of the piston nose at different points.

Figure 21 shows the Mach number in the orifice at the same times previously mentioned. The region of the highest Mach number is in the throat of the orifice, as expected. The acceleration and deceleration of the LP entering and exiting the orifice can be seen. As with shot 38, there is no tendency of the flow to separate from the piston surfaces, indicating a well-designed orifice.

6. Conclusions

The DSD/SST-based finite element model of the injection of the LP through the orifice in the RLPG was described. The model was used to simulate shot 38 of the 30-mm RLPG. The reservoir pressure and injection piston motion computed by the model compare well with the values coming from a lumped parameter simulation of the shot. Also, the discharge

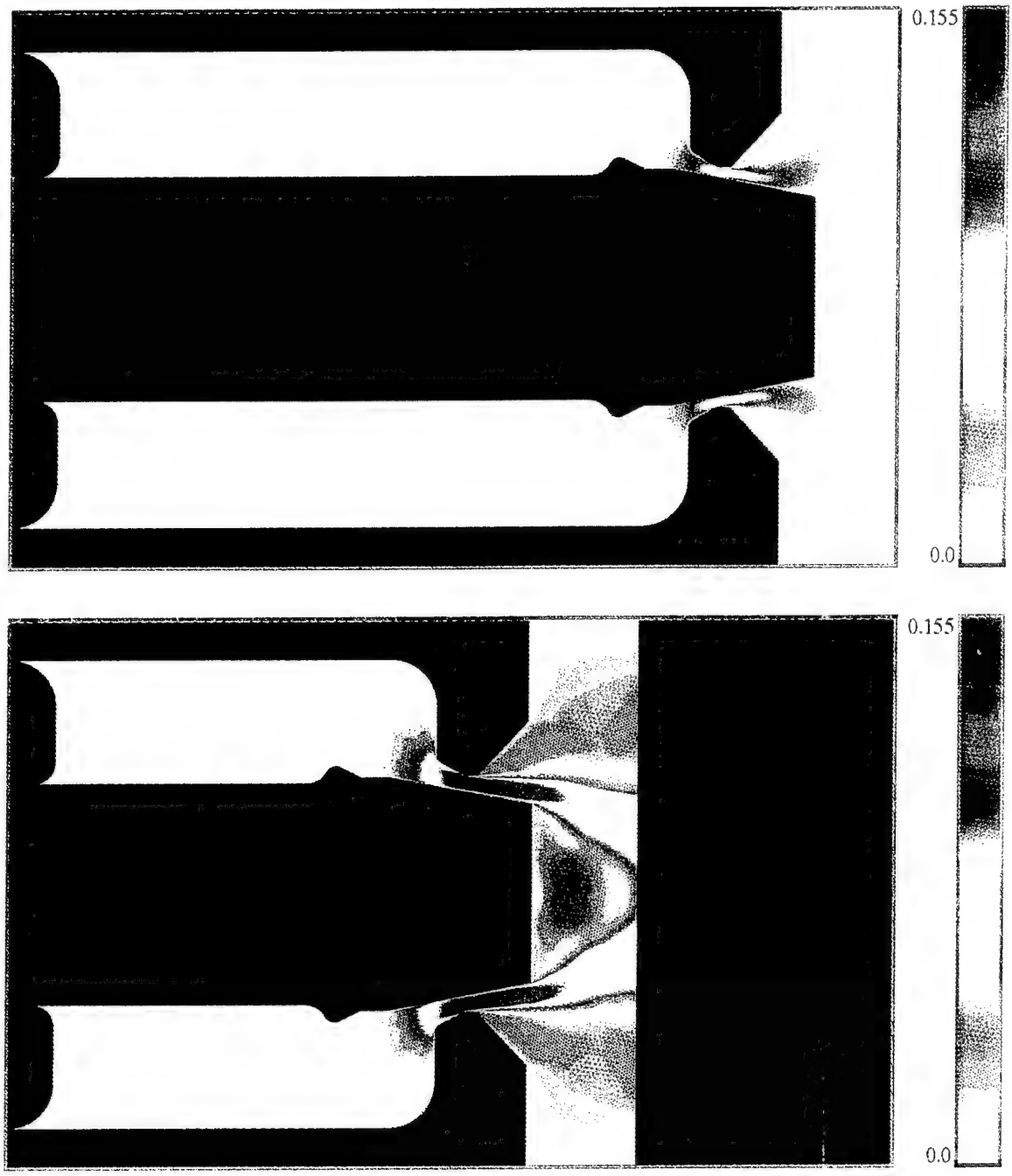

Figure 19. Shot 128: Global View of Mach Number Contours at Times 10.0 ms and 12.0 ms.

coefficient is reasonably close to the expected value. Because of this agreement, the data generated by the model can be taken as at least qualitatively correct. A total of three shots of the 30-mm RLPG were studied.

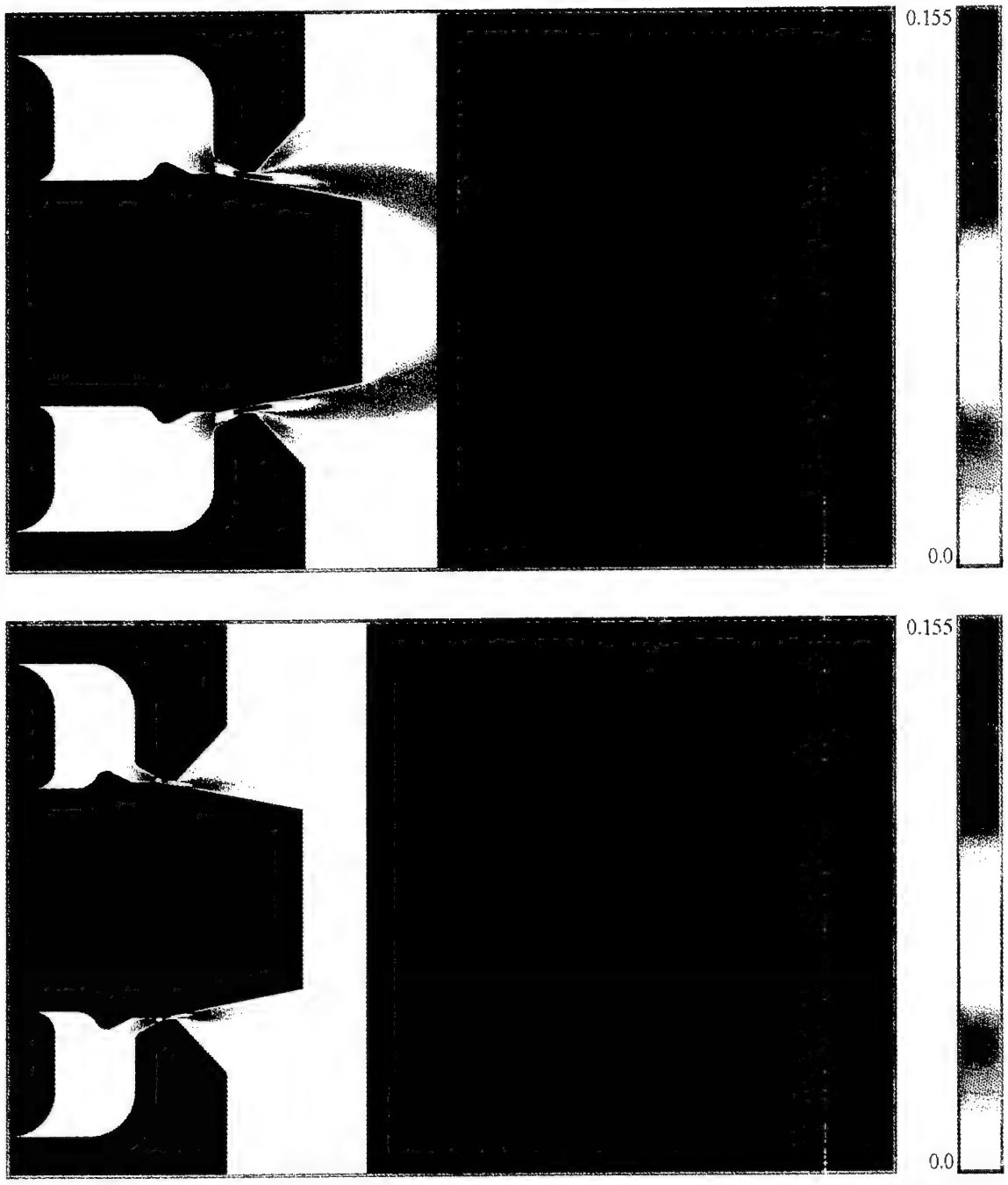

Figure 20. Shot 128: Global View of Mach Number Contours at Times 14.0 ms and 16.0 ms.

Shot 38 was a small-charge shot, and shot 128 was a medium-charge shot. The RLPG performed properly during both of these shots. The flow of LP through the orifice tended to remain attached to both pistons through the orifice and to the control piston into the

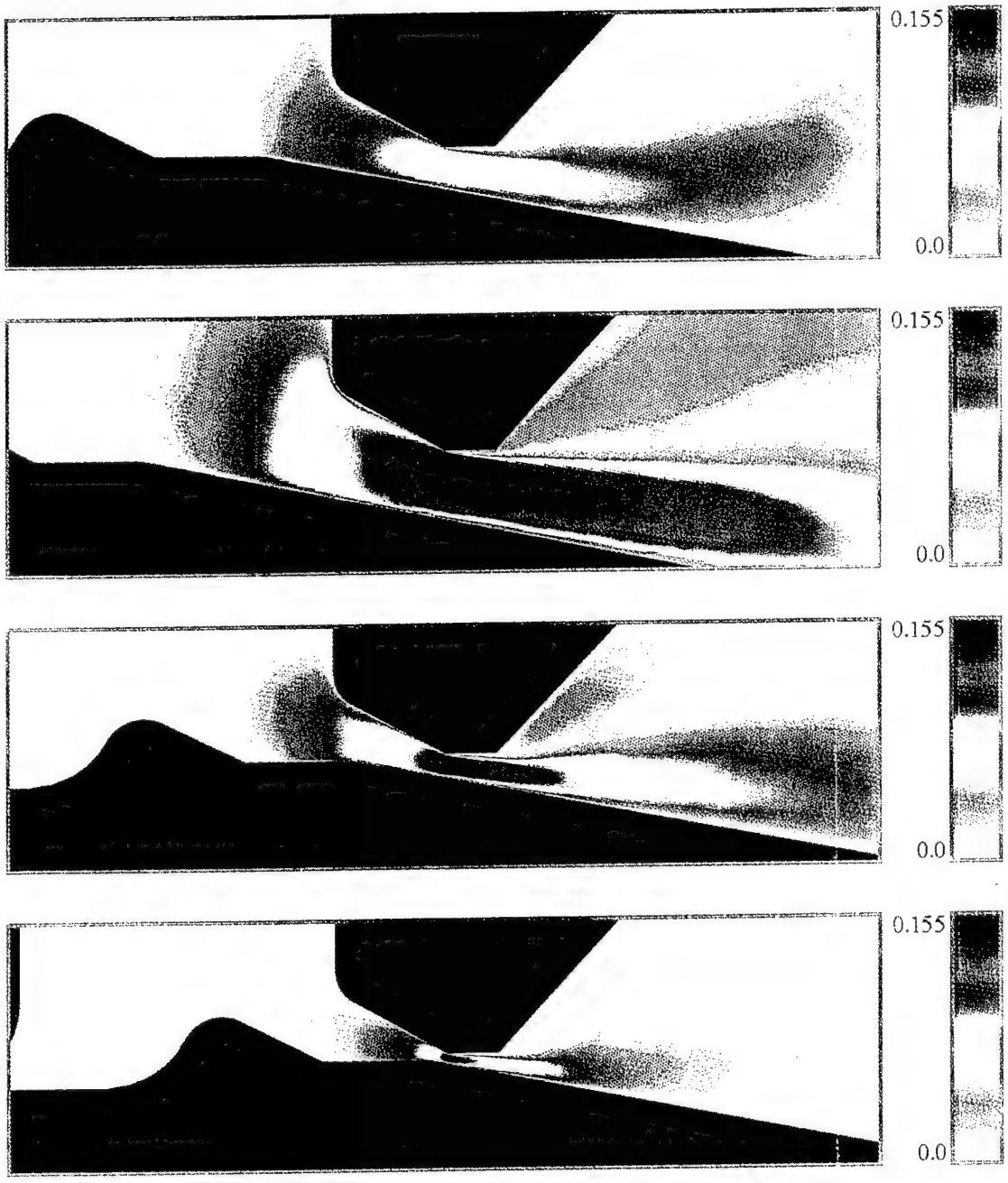

Figure 21. Shot 128: Mach Number Contours in the Orifice at Times 10.0 ms, 12.0 ms, 14.0 ms, and 16.0 ms.

combustion chamber. The point where the jet lifted off of the control piston differed between the shots and varied during the firing cycle. The behavior of the jet in the chamber is not to be considered very accurate, since combustion strongly influences the flow in the chamber. The flow in the orifice behaves well, indicating that the orifice is well designed.

This work provides confidence that the model can be used to study the flow of LP from the reservoir and through the orifice. However, since it neglects combustion, the model cannot predict phenomena that occur in the chamber. A current project involves the coupling of the reservoir model with a model of the chamber, which includes combustion. The resulting model will be used to study the entire firing cycle of the RLPG.

INTENTIONALLY LEFT BLANK.

7. References

1. Coffee, T. P., G. P. Wren, and W. F. Morrison. "A Comparison Between Experiment and Simulation for Concept VIC Regenerative Liquid Propellant Guns. I. 30 mm." BRL-TR-3072, U.S. Army Ballistic Research Laboratory, Aberdeen Proving Ground, MD, 1989.

2. Coffee, T. P. "A Lumped Parameter Code for Regenerative Liquid Propellant Guns." BRL-TR-2703, U.S. Army Ballistic Research Laboratory, Aberdeen Proving Ground, MD, 1985.

3. Coffee, T. P. "One-Dimensional Modeling of Liquid Injection in a Regenerative Propellant Gun." BRL-TR-2897, U.S. Army Ballistic Research Laboratory, Aberdeen Proving Ground, MD, 1988.

4. Coffee, T. P., P. G. Baer, W. F. Morrison, and G. P. Wren. "Jet Breakup and Combustion Modeling for the Regenerative Liquid Propellant Gun." BRL-TR-3223, U.S. Army Ballistic Research Laboratory, Aberdeen Proving Ground, MD, 1991.

5. Coffee, T. P. "A Two-Dimensional Model for Pressure Oscillations: Extension to Generalized Geometry." ARL-TR-349, U.S. Army Research Laboratory, Aberdeen Proving Ground, MD, 1994.

6. Coffee, T. P. "A Two-Dimensional Model for the Combustion Chamber/Gun Tube of a Concept VIC Regenerative Liquid Propellant Gun." BRL-TR-3341, U.S. Army Ballistic Research Laboratory, Aberdeen Proving Ground, MD, 1992.

7. Wren, G. P., S. E. Ray, S. K. Aliabadi, and T. E. Tezduyar. "Space-Time Finite Element Computation of Compressible Flows Between Moving Components." *International Journal for Numerical Methods in Fluids*, vol. 21, pp. 981–991, 1995.

8. Tezduyar, T. E., M. Behr, and J. Liou. "A New Strategy for Finite Element Computations Involving Moving Boundaries and Interfaces – the Deforming-Spatial-Domain/Space-Time Procedure: I. The Concept and the Preliminary Tests." *Computer Methods in Applied Mechanics and Engineering*, vol. 94, pp. 339–351, 1992.

9. Tezduyar, T. E., M. Behr, S. Mittal, and J. Liou. "A New Strategy for Finite Element Computations Involving Moving Boundaries and Interfaces – the Deforming-Spatial-Domain/Space-Time Procedure: II. Computation of Free-Surface Flows, Two-Liquid Flows, and Flows with Drifting Cylinders." *Computer Methods in Applied Mechanics and Engineering*, vol. 94, pp. 353–371, 1992.

10. Aliabadi, S. K. and T. E. Tezduyar. "Space-Time Finite Element Computation of Compressible Flows Involving Moving Boundaries and Interfaces." *Computer Methods in Applied Mechanics and Engineering*, vol. 107, pp. 209–224, 1993.

11. Brooks, A. N. and T. J. R. Hughes. "Streamline Upwind/Petrov-Galerkin Formulations for Convection Dominated Flows with Particular Emphasis on the Incompressible Navier-Stokes Equations." *Computer Methods in Applied Mechanics and Engineering*, vol. 32, pp. 199–259, 1982.

12. Le Beau, G. J., S. E. Ray, S. K. Aliabadi, and T. E. Tezduyar. "SUPG Finite Element Computation of Compressible Flows with the Entropy and Conservation Variables Formulations." *Computer Methods in Applied Mechanics and Engineering*, vol. 104, pp. 397–422, 1993.

13. Aliabadi, S. K., S. E. Ray, and T. E. Tezduyar. "SUPG Finite Element Computation of Viscous Compressible Flows based on the Conservation and Entropy Variables Formulations." *Computational Mechanics*, vol. 11, pp. 300–312, 1993.

14. Hughes, T. J. R. and M. Mallet. "A New Finite Element Formulation for Computational Fluid Dynamics: IV. A Discontinuity-Capturing Operator for Multidimensional Advective-Diffusive Systems." *Computer Methods in Applied Mechanics and Engineering*, vol. 58, pp. 329–339, 1986.

15. Aliabadi, S. K. and T. E. Tezduyar. "Massively Parallel Compressible Flow Computations in Aerospace Applications." *Extended Abstracts of the Second Japan-US Symposium on Finite Element Methods in Large-Scale Computational Fluid Dynamics*, Tokyo, Japan, 1994.

16. Johnson, A. A. *Mesh Generation and Update Strategies for Parallel Computation of Flow Problems with Moving Boundaries and Interfaces.* Ph.D. thesis, Department of Aerospace Engineering and Mechanics, University of Minnesota, 1995.

17. Ray, S. E. *Large-Scale Computational Strategies for Solving Compressible Flow Problems.* Ph.D. thesis, Department of Aerospace Engineering and Mechanics, University of Minnesota, 1995.

18. Johnson, A. A. and T. E. Tezduyar. "Mesh Update Strategies in Parallel Finite Element Computations of Flow Problems with Moving Boundaries and Interfaces." *Computer Methods in Applied Mechanics and Engineering*, vol. 119, pp. 73–94, 1994.

19. Saad, Y. and M. Schultz. "GMRES: A Generalized Minimal Residual Algorithm for Solving Nonsymmetric Linear Systems." *SIAM Journal of Scientific and Statistical Computing*, vol. 7, pp. 856–869, 1986.

20. Colburn, J. W. Private communication. U.S. Army Research Laboratory, Aberdeen Proving Ground, MD, 1997.

NO. OF COPIES	ORGANIZATION
2	DEFENSE TECHNICAL INFORMATION CENTER DTIC DDA 8725 JOHN J KINGMAN RD STE 0944 FT BELVOIR VA 22060-6218
1	HQDA DAMO FDQ DENNIS SCHMIDT 400 ARMY PENTAGON WASHINGTON DC 20310-0460
1	CECOM SP & TRRSTRL COMMCTN DIV AMSEL RD ST MC M H SOICHER FT MONMOUTH NJ 07703-5203
1	PRIN DPTY FOR TCHNLGY HQ US ARMY MATCOM AMCDCG T M FISETTE 5001 EISENHOWER AVE ALEXANDRIA VA 22333-0001
1	PRIN DPTY FOR ACQUSTN HQS US ARMY MATCOM AMCDCG A D ADAMS 5001 EISENHOWER AVE ALEXANDRIA VA 22333-0001
1	DPTY CG FOR RDE HQS US ARMY MATCOM AMCRD BG BEAUCHAMP 5001 EISENHOWER AVE ALEXANDRIA VA 22333-0001
1	DPTY ASSIST SCY FOR R&T SARD TT T KILLION THE PENTAGON WASHINGTON DC 20310-0103
1	OSD OUSD(A&T)/ODDDR&E(R) J LUPO THE PENTAGON WASHINGTON DC 20301-7100

NO. OF COPIES	ORGANIZATION
1	INST FOR ADVNCD TCHNLGY THE UNIV OF TEXAS AT AUSTIN PO BOX 202797 AUSTIN TX 78720-2797
1	DUSD SPACE 1E765 J G MCNEFF 3900 DEFENSE PENTAGON WASHINGTON DC 20301-3900
1	USAASA MOAS AI W PARRON 9325 GUNSTON RD STE N319 FT BELVOIR VA 22060-5582
1	CECOM PM GPS COL S YOUNG FT MONMOUTH NJ 07703
1	GPS JOINT PROG OFC DIR COL J CLAY 2435 VELA WAY STE 1613 LOS ANGELES AFB CA 90245-5500
1	ELECTRONIC SYS DIV DIR CECOM RDEC J NIEMELA FT MONMOUTH NJ 07703
3	DARPA L STOTTS J PENNELLA B KASPAR 3701 N FAIRFAX DR ARLINGTON VA 22203-1714
1	SPCL ASST TO WING CMNDR 50SW/CCX CAPT P H BERNSTEIN 300 O'MALLEY AVE STE 20 FALCON AFB CO 80912-3020
1	USAF SMC/CED DMA/JPO M ISON 2435 VELA WAY STE 1613 LOS ANGELES AFB CA 90245-5500

NO. OF
COPIES ORGANIZATION

1 US MILITARY ACADEMY
MATH SCI CTR OF EXCELLENCE
DEPT OF MATHEMATICAL SCI
MDN A MAJ DON ENGEN
THAYER HALL
WEST POINT NY 10996-1786

1 DIRECTOR
US ARMY RESEARCH LAB
AMSRL CS AL TP
2800 POWDER MILL RD
ADELPHI MD 20783-1145

1 DIRECTOR
US ARMY RESEARCH LAB
AMSRL CS AL TA
2800 POWDER MILL RD
ADELPHI MD 20783-1145

3 DIRECTOR
US ARMY RESEARCH LAB
AMSRL CI LL
2800 POWDER MILL RD
ADELPHI MD 20783-1145

ABERDEEN PROVING GROUND

3 DIR USARL
AMSRL CI LP (305)

NO. OF COPIES	ORGANIZATION
1	CDR US ARMY ARDEC AMSTA AR AEE B D DOWNS PICATINNY ARSENAL NJ
3	CDR US ARMY ARDEC AMSTA AR FSS DA R KOPMANN B MACHEK J IRIZARRY PICATINNY ARSENAL NJ 07806-5000
1	DIRECTOR BENET WEAPONS LAB AMSTA AR CCB RA G P OHARA WATERVLIET NY 12189-4050
2	CDR US ARMY RSRCH OFC TECH LIBRARY D MANN PO BOX 12211 RESEARCH TRIANGLE PARK NC 27709-2211
1	COMMANDANT US ARMY COMMAND AND GENERAL STAFF COLLEGE FORT LEAVENWORTH KS 66027
1	CDR US ARMY FOREIGN SCI & TECH CTR AMXST MC 3 220 SEVENTH ST NE CHARLOTTESVILLE VA 22901-5396
2	CDR HQ AMCCOM AMSMC LSL B KELEBER AMSMC SAS WF G SCHELENKER ROCK ISLAND IL 61299-6000
1	CDR NASC AIR 954 TECH LIBRARY WASHINGTON DC 20360
1	CDR NRL RSRCH LIBRARY CODE 5220 WASHINGTON DC 20375-5000

NO. OF COPIES	ORGANIZATION
1	OFFICE OF NAVAL RSRCH CODE 473 R S MILLER 800 N QUINCY ST ARLINGTON VA 22217-9999
1	CDR NSWC CODE G30 GUNS & MUNITIONS DIV DAHLGREN VA 22448-5000
1	CDR NSWC CODE G32 GUNS SYSTEMS DIV DAHLGREN VA 22448-5000
1	CDR NSWC CODE E23 TECH LIBRARY DAHLGREN VA 22448-5000
1	CDR NAWC INFO SCIENCE DIV CHINA LAKE CA 93555-6001
1	COMMANDING OFFICER NAVAL UNDERWATER SYS CTR CODE 5B331 TECH LIBRARY NEWPORT RI 02840
3	AL LSCF J LEVINE L QUINN T EDWARDS EDWARDS AIR FORCE BASE CA 93523-5000
2	NASA LANGLEY RSRCH CTR MS 408 W SCALLION D WITCOFSKI HAMPTON VA 23605
1	DIRECTOR SANDIA NATIONAL LAB R CARLING COMBUSTION RSRCH FACILITY LIVERMORE CA 94551-0469

NO. OF COPIES	ORGANIZATION
1	DIR LLNL L355 M FINGER PO BOX 808 LIVERMORE CA 94550-0622
1	DIRECTOR LOS ALAMOS SCI LAB T3 D BUTLER PO BOX 1663 LOS ALAMOS NM 87544
1	INST FOR DEFENSE ANALYSES D SPARROW 1801 N BEAUREGARD ST ALEXANDRIA VA 22311-1772
1	PAUL GOUGH ASSOC P S GOUGH 1048 SOUTH ST PORTSMOUTH NH 03801-5423
1	PHYSICS INTERNATIONAL LIBRARY H WAYNE WAMPLER PO BOX 5010 SAN LEANDRO CA 94577-0599
1	GENERAL DYNAMICS DFNS SYS PCRL DIV N A MESSINA PRINCETON CORPORATE PLAZA 11 DEERPARK DR BLDG IV SUITE 119 MONMOUTH JUNCTION NJ 08852
1	VERITAY TECH INC E FISHER 4845 MILLERSPORT HWY EAST AMHERST NY 14501-0305
1	SRI INTERNATIONAL TECH LIBRARY PROPULSION SCIENCES DIV 333 RAVENWOOD AVE MENLO PARK CA 94025-3493

NO. OF COPIES	ORGANIZATION
6	GENERAL DYNAMICS DFNS SYS G KEELER T KURIATA B FEATHEROFF I MAGOON M TWEED-KENT C BANKER 100 PLASTICS AVE PITTSFIELD MA 01201-3698
3	COMBUSTION RSRCH & FLOW TECH INC S DASH A HOSANGADI N SINHA 174 N MAIN ST BLDG 3 PO BOX 1150 DUBLIN PA 18917
1	THE PENNA STATE UNIV DEPT OF MECH ENG K K KUO 140 RESEARCH BLDG EAST UNIVERSITY PARK PA 16802
1	THE PENNA STATE UNIV DEPT OF MECH ENG S T THYNELL 309 REBER BLDG UNIVERSITY PARK PA 16802
1	UNIV OF MINNESOTA ARMY HPC RSRCH CTR T E TEZDUYAR 1100 WASHINGTON AVE S SUITE 101 MINNEAPOLIS MN 55415
2	DIRECTOR DEFENSE ADVANCED RSRCH PROJECTS AGENCY J LUPO J RICHARDSON 1400 WILSON BLVD ARLINGTON VA 22209

NO. OF COPIES	ORGANIZATION
1	SUPERINTENDENT NAVAL POSTGRAD SCHOOL DEPT OF MECH ENG CODE 1424 LIBRARY MONTEREY CA 93943
1	DIRECTOR JET PROPULSION LAB TECH LIBRARY 4800 OAK GROVE DR PASADENA CA 91109
2	DIRECTOR NAT AERONAUTICS & SPACE ADMIN MS 603 TECH LIBRARY MS 86 DR POVINELLI 21000 BROOKPARK RD LEWIS RSRCH CTR CLEVELAND OH 44135
	ABERDEEN PROVING GROUND
31	DIR USARL AMSRL WM P A HORST AMSRL WM PA T COFFEE G WREN (2 CPS) A BIRK J DESPIRITO J KNAPTON C LEVERITT T MINOR W OBERLE P TRAN L-M CHANG J COLBURN P CONROY G KELLER D KOOKER T ROSENBERGER M NUSCA S RAY (10 CPS) AMSRL WM PB P PLOSTINS AMSRL WM PC B FORCH AMSRL WM PD B BURNS

NO. OF
COPIES ORGANIZATION

1 MR CLIVE WOODLEY
BLDG R31
WXG GUN SYSTEMS DEPT
DERA FORT HALSTEAD
SEVENOAKS KENT TN14 7BP
UNITED KINGDOM

1 DEFENCE SCIENCE & TECH ORGN
WEAPON SYSTEMS DIVISION
ANNA WILDEGGER-GAISSMAIER
PO BOX 1500
SALISBURY SOUTH AUSTRALIA 5108
AUSTRALIA

REPORT DOCUMENTATION PAGE

Form Approved
OMB No. 0704-0188

1. AGENCY USE ONLY *(Leave blank)*	2. REPORT DATE	3. REPORT TYPE AND DATES COVERED
	September 1997	Summary, June 1993 - February 1995

4. TITLE AND SUBTITLE
A Numerical Study of the Injector Region of the 30-mm Regenerative Liquid Propellant Gun

5. FUNDING NUMBERS
1L16261B41FL

6. AUTHOR(S)
S. E. Ray

7. PERFORMING ORGANIZATION NAME(S) AND ADDRESS(ES)
U.S. Army Research Laboratory
ATTN: AMSRL-WM-PA
Aberdeen Proving Ground, MD 21005-5066

8. PERFORMING ORGANIZATION REPORT NUMBER
ARL-CR-336

9. SPONSORING/MONITORING AGENCY NAMES(S) AND ADDRESS(ES)

10.SPONSORING/MONITORING AGENCY REPORT NUMBER

11. SUPPLEMENTARY NOTES

12a. DISTRIBUTION/AVAILABILITY STATEMENT
Approved for public release; distribution is unlimited.

12b. DISTRIBUTION CODE

13. ABSTRACT *(Maximum 200 words)*

A numerical study of the flow of liquid propellant (LP) in a regenerative LP gun (RLPG) is described. The model simulates the flow of LP from the liquid reservoir, through the orifice, and into the combustion chamber. The model is based on a space-time finite element method and can automatically handle the deformation of the computational domain. A mesh-moving scheme is used to update the mesh at every time step.

Two shots of the 30-mm RLPG are studied. One is a small-charge shot, and the other is a medium-charge shot. The results from the simulations compare well with data from another numerical model of the RLPG and with experimental data. The simulations provide qualitative details of the transient phenomena that occur in the orifice during the firing cycle. The agreement of the results from the model with experimental data provide confidence in the accuracy of the model. The numerical model will be used to study several RLPG shots under a variety of conditions.

14. SUBJECT TERMS
liquid propellant, numerical modeling, finite element

15. NUMBER OF PAGES
48

16. PRICE CODE

17. SECURITY CLASSIFICATION OF REPORT	18. SECURITY CLASSIFICATION OF THIS PAGE	19. SECURITY CLASSIFICATION OF ABSTRACT	20. LIMITATION OF ABSTRACT
UNCLASSIFIED	UNCLASSIFIED	UNCLASSIFIED	UL

INTENTIONALLY LEFT BLANK.

USER EVALUATION SHEET/CHANGE OF ADDRESS

This Laboratory undertakes a continuing effort to improve the quality of the reports it publishes. Your comments/answers to the items/questions below will aid us in our efforts.

1. ARL Report Number/Author ARL-CR-336 (Ray [POC: W. Sturek]) Date of Report September 1997

2. Date Report Received _____

3. Does this report satisfy a need? (Comment on purpose, related project, or other area of interest for which the report will be used.) _____

4. Specifically, how is the report being used? (Information source, design data, procedure, source of ideas, etc.) _____

5. Has the information in this report led to any quantitative savings as far as man-hours or dollars saved, operating costs avoided, or efficiencies achieved, etc? If so, please elaborate. _____

6. General Comments. What do you think should be changed to improve future reports? (Indicate changes to organization, technical content, format, etc.) _____

CURRENT ADDRESS

_____
Organization

_____
Name E-mail Name

_____
Street or P.O. Box No.

_____
City, State, Zip Code

7. If indicating a Change of Address or Address Correction, please provide the Current or Correct address above and the Old or Incorrect address below.

OLD ADDRESS

_____
Organization

_____
Name

_____
Street or P.O. Box No.

_____
City, State, Zip Code

(Remove this sheet, fold as indicated, tape closed, and mail.)
(DO NOT STAPLE)